

<i>CONTENTS</i>	1
<b>Contents</b>	
<b>1 Introduction</b>	<b>3</b>
1.1 Heterogeneous Catalysis and Irreversible Reaction Processes . . . . .	4
1.2 Absorbing States and Irreversible Phase Transitions (IPT's) . . . . .	6
<b>2 Theoretical Approaches</b>	<b>9</b>
2.1 The Monte Carlo Method . . . . .	10
2.1.1 The Standard Ensemble . . . . .	11
2.1.2 The Constant Coverage Ensemble . . . . .	12
2.1.3 Finite-Size Scaling Approach to Second-Order IPT's . . . . .	13
2.1.4 The Epidemic Method and Dynamic Scaling . . . . .	14
2.2 Analytical Methods . . . . .	16
2.2.1 The Langevin Formulation . . . . .	17
2.2.2 Mean-Field Treatments . . . . .	19
<b>3 Critical Behaviour of Specific Reaction Systems</b>	<b>20</b>
3.1 The Catalytic Oxidation of Carbon Monoxide . . . . .	20
3.2 The Catalytic Reaction Between Nitrogen Monoxide and Carbon Monoxide.	41
3.3 Brief Overview of Other Surface Reaction Processes . . . . .	49
<b>4 Conclusions</b>	<b>51</b>
<b>5 References</b>	<b>53</b>

# Critical Behaviour of Irreversible Reaction Systems

**Ernesto Loscar and Ezequiel V. Albano**

Instituto de Investigaciones Fisicoquímicas Teóricas y Aplicadas (INIFTA)  
Sucursal 4, Casilla de Correo 16. (1900) La Plata  
Argentina

**Abstract.** An introductory review on the critical behaviour of some irreversible reaction systems is given. The study of these systems has attracted great attention during the last decades due to, on the one hand, the rich and complex underlying physics, and on the other hand, their relevance for numerous technological applications in heterogeneous catalysis, corrosion and coating, development of microelectronic devices, etc.. The review is focused on recent advances in the understanding of irreversible phase transitions (IPT's) providing a survey of the theoretical development of the field during the last decade, as well as a detailed discussion of relevant numerical simulations. The Langevin formulation for the treatment of second-order IPT's is discussed. Different Monte Carlo approaches are also presented in detail and the finite-size scaling analysis of second-order IPT's is described. Special attention is devoted to the description of recent progress in the study of first-order IPT's observed upon catalytic oxidation of carbon monoxide and the reduction of nitrogen monoxide, using lattice gas reaction models. Only brief comments are given on other reactions such as the oxidation of hydrogen, ammonia synthesis, etc. Also, a discussion of relevant experiments is presented and measurement are compared with the numerical results. Furthermore, promising areas for further research and open questions are also addressed.

## 1. Introduction

The study and understanding of heterogeneously catalyzed reactions is a field that contains an enormous wealth of still unclear or even completely unexplained phenomena. This scenario leads to an exciting and challenging domain for investigation and fundamental research. Furthermore, the occurrence of many complex and fascinating physical and chemical phenomena, such as pattern formation and self-organization [1, 2], regular and irregular kinetic oscillations [1, 2, 3, 4, 5, 6], propagation and interference of chemical waves and spatio-temporal structures [7, 8], the transition into chaotic behaviour [9, 10], fluctuation-induced transitions [11], irreversible phase transitions (IPT's) [12, 13, 14, 15, 16], etc, has attracted the attention of many scientists.

In addition to the basic interest, heterogeneous catalysis is a field of central importance for numerous industrial (e.g. synthesis of ammonia, sulfuric and nitric acids, cracking and reforming processes of hydrocarbons, etc.) and practical (e.g. catalytic control of environmental pollution such as the emission of  $CO$ ,  $NO_x$ ,  $SO_2$ ,  $O_3$ , etc.) applications. Furthermore, information technology, material science, corrosion, energy conversion, ecology and environmental sciences, etc. are some fields whose rapid growth is somehow based on the recent progress in the study of heterogeneous reactions occurring on surfaces and interfaces.

It should be noticed that recent developments of experimental techniques such as Scanning Tunneling Microscopy (STM), Low Energy Electron Diffraction (LEED), High Resolution Electron Energy Loss Spectroscopy (HREELS), Ultraviolet Photoelectric Spectroscopy (UPS), Photoelectron Emission Microscopy (PEEM), etc. [17, 18, 19], just to quote few of them, allows the scientists to gather detailed physical and chemical information about surfaces, adsorbates and reaction products. Within this context, the STM based measurement of the reaction rate parameters at a microscopic level for the catalytic oxidation of  $CO$  [20] is a clear example of the progress recently achieved. Remarkably, the measured parameters agree very well with those previously obtained by means of macroscopic measurements. Also, all elementary steps of a chemical reaction have been induced on individual molecules in a controlled step-by-step manner with the aid of STM techniques [21]. Furthermore, very recently, the oxidation of  $CO$  on  $Pt(110)$  was studied by means of STM techniques inside a high-pressure flow reactor, i.e. under semirealistic conditions as compared with those prevailing in the actual catalytic process [22]. It is interesting to notice that a new reaction mechanism, not observed when the

reaction takes place under low pressure, has been identified [22]. Due to this stimulating generation of accurate experimental information, the study of catalyzed reaction systems is certainly a challenging scientific field for the development and application of analytical methods, theories and numerical simulations.

Within this context, the aim of this report is to review recent progress in the understanding of IPT's occurring in various lattice gas reaction systems (LGRS). It should be noticed that LGRS models are crude approximations of the actual (very complex) catalytic processes. However, from the physicist's point of view, the LGRS approach is widely used because it is very useful to gain insight into far-from equilibrium processes. In fact, due to the lack of a well-established theoretical framework, unlike the case of their equilibrium counterpart, the progress of the statistical mechanics of systems out of equilibrium relies, up to some extent, on the study and understanding of simple models. So, in the case of LGRS, one renounces to a detailed description of the catalyzed reaction and, instead, the interest is focused on the irreversible critical behaviour of archetype models inspired in the actual reaction systems.

Keeping these concepts in mind, the review will be devoted to survey the theoretical development of the field during the last decade and to discuss promising areas for further research as well as open questions.

### *1.1. Heterogeneous Catalysis and Irreversible Reaction Processes*

In most cases, heterogeneously catalyzed reactions proceed according to well-established elementary steps. The first one comprises trapping, sticking and adsorption. Gaseous reactant atoms and/or molecules are trapped by the potential well of the surface. This rather weak interaction is commonly considered as a physisorbed precursor state. Subsequently, species are promoted to the chemisorbed state where a much stronger interaction potential is activated. Particularly important from the catalytic point of view is that molecules frequently undergo dissociation, e.g.  $N_2$ ,  $O_2$ ,  $H_2$ , etc, which is a process that frees highly reactive atomic species on the surface. Sticking and adsorption processes depend on the surface structure (both geometric and electronic). In some cases, chemisorption of small atoms and molecules may induce the reconstruction of the surface. This effect, coupled to structure dependent sticking coefficients, may lead to the occurrence of collective phenomena such as oscillations [3, 4, 5].

After adsorption, species may diffuse on the surface or, eventually, become absorbed in the bulk. Due to collisions between adsorbed species of different kind the actual

reaction step can occur. Of course, this step requires that energetic and spatial constraints be fulfilled. The result of the reaction step is the formation of a product molecule. This product can be either an intermediate of the reaction or its final output.

The final step of the whole reaction process is the desorption of the products. This step is essential not only for the practical purpose of collecting and storing the desired output, but also for the regeneration of the catalytic active sites of the surface. Most reactions have at least one rate limiting step, which frequently makes the reaction prohibitively slow for practical purposes when, for instance, it is intended in an homogeneous (gas or fluid) medium. The role of a good solid-state catalyst is to obtain acceptable output rate of the products. Reactions occurring in this way are commonly known as heterogeneously catalyzed.

At this stage and in order to illustrate the above-mentioned elementary steps, it is useful to point our attention to a specific reaction system. For this purpose, the catalytic oxidation of carbon monoxide, namely  $2CO + O_2 \rightarrow 2CO_2$ , which is likely the most studied reaction system, has been selected. It is well known that such reaction proceeds according to the Langmuir-Hinshelwood mechanism [23, 24], i.e with both reactants adsorbed on the catalyst's surface



where  $S$  is an empty site on the surface, while  $(a)$  and  $(g)$  refer to the adsorbed and gas phase, respectively. The reaction takes place with the catalyst, e.g  $Pt$ , in contact with a reservoir of  $CO$  and  $O_2$  whose partial pressures are  $P_{CO}$  and  $P_{O_2}$ , respectively.

Equation (1) describes the irreversible molecular adsorption of  $CO$  on a single site of the catalyst's surface. It is known that at under suitable temperature and pressure reaction conditions,  $CO$  molecules diffuse on the surface. Furthermore, there is a small probability of  $CO$  desorption that increases as the temperature is raised [3].

Equation (2) corresponds to the irreversible adsorption of  $O_2$  molecules that involves the dissociation of such species and the resulting  $O$  atoms occupy two sites of the catalytic surface. Under reaction conditions both the diffusion and the desorption of oxygen are negligible. Due to the high stability of the  $O_2$  molecule the whole reaction does not occur in the homogeneous phase due to the lack of  $O_2$  dissociation. So, equation

(2) dramatically shows the role of the catalyst that makes feasible the rate limiting step of the reaction.

Finally, equation (3) describes the formation of the product ( $CO_2$ ) that desorbs from the catalyst's surface. This final step is essential for the regeneration of the catalytic active surface.

### 1.2. Absorbing States and Irreversible Phase Transitions (IPT's)

Assuming irreversible adsorption-reaction steps, as in the case of equations (1-3), it may be expected that on the limit of large  $P_{CO}$  and small  $P_{O_2}$  (small  $P_{CO}$  and large  $P_{O_2}$ ) values, the surface of the catalyst would become saturated by  $CO$  ( $O_2$ ) species and the reaction would stop. In fact, the surface of the catalyst fully covered by a single type of species, where further adsorption of the other species is no longer possible, corresponds to an inactive state of the system. This state is known as 'poisoned', in the sense that adsorbed species on the surface of the catalyst are the poison that causes the reaction to stop. Physicists used to call such state (or configuration) 'absorbing' because a system can be trapped by it forever, with no possibility of escape [25].

These concepts are clearly illustrated in figure 1, which shows plots of the rate of  $CO_2$  production ( $R_{CO_2}$ ) and the surface coverage with  $CO$  and  $O_2$  ( $\theta_{CO}$  and  $\theta_O$ , respectively), versus the partial pressure of  $CO$  ( $P_{CO}$ ), as obtained using the Ziff-Gulari-Barshad (ZGB) lattice gas reaction model [26]. Details on the ZGB model will be discussed extensively below, see also [15, 16]. For  $P_{CO} \leq P_{1CO} \cong 0.38975$  the surface becomes irreversibly poisoned by  $O$  species with  $\theta_{CO} = 0$ ,  $\theta_O = 1$  and  $R_{CO_2} = 0$ . In contrast, for  $P_{CO} \geq P_{2CO} \cong 0.5255$  the catalyst is irreversibly poisoned by  $CO$  molecules with  $\theta_{CO} = 1$ ,  $\theta_O = 0$  and  $R_{CO_2} = 0$ . These poisoned states are absorbing and the system cannot escape from them. However, as shown in figure 1, between these absorbing states there is a reaction window, namely for  $P_{1CO} < P_{CO} < P_{2CO}$ , such that a steady state with sustained production of  $CO_2$  is observed.

It is worth mentioning that starting from the reactive regime and approaching the oxygen absorbing state, all quantities of interest change smoothly until they adopt the values corresponding to the absorbing state. This behaviour typically corresponds to a second-order irreversible phase transition (IPT). The transition is irreversible because when the control parameter ( $P_{CO}$  in this example) is tuned into the absorbing state the system becomes trapped by it forever. This behaviour is in contrast to that observed for second-order reversible phase transitions, such as the order-disorder transition of

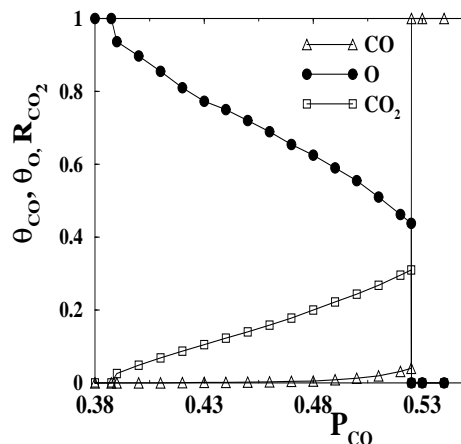


**Figure 1.** Phase diagram of the ZGB model obtained using the Standard Ensemble, showing the dependence of the surface coverage with  $CO$  ( $\theta_{CO}$ ) and Oxygen ( $\theta_O$ ), and the rate of  $CO_2$  production ( $R_{CO_2}$ ) on the partial pressure of  $CO$  ( $P_{CO}$ ) in the gas phase. Irreversible phase transitions occurring at  $P_{1CO} \simeq 0.38975$  (second-order) and  $P_{2CO} \simeq 0.5255$  (first-order) can clearly be observed.

the Ising ferromagnet in the absence of an external magnetic field, where it is possible to change reversibly from one phase to the other, simply tuning the control parameter [27, 28]. For second-order IPT's, as in the case of their reversible counterparts, it is possible to define an order parameter, which for the former is given by the concentration of minority species ( $\theta_{CO}$ , in the case of the second-order IPT of the catalytic oxidation of  $CO$ ). Furthermore, it is known that  $\theta_{CO}$  vanishes according to a power law upon approaching the critical point [29], so that

$$\theta_{CO} \propto (P_{CO} - P_{1CO})^\beta, \quad (4)$$

where  $\beta$  is the order parameter critical exponent and  $P_{1CO}$  is the critical point.

Remarkably, the behaviour of the system is quite different upon approaching the  $CO$  absorbing state from the reactive regime (see figure 1). In this case, all quantities of interest exhibit a marked discontinuity close to  $P_{2CO} \cong 0.5255$ . This is a typical first-order IPT and  $P_{2CO}$  is the coexistence point.

Experimental results for the catalytic oxidation of carbon monoxide on  $Pt(210)$  and  $Pt(111)$  [18, 19] are in qualitative agreement with simulation results of the ZGB model, it follows from the comparison of figures 1 and 2. A remarkable agreement is the (almost) linear increase in the reaction rate observed when the  $CO$  pressure is raised and the abrupt drop of the reactivity when a certain 'critical' pressure is reached. In spite of the similarities observed, two essential differences are worth discussing: i) the oxygen-

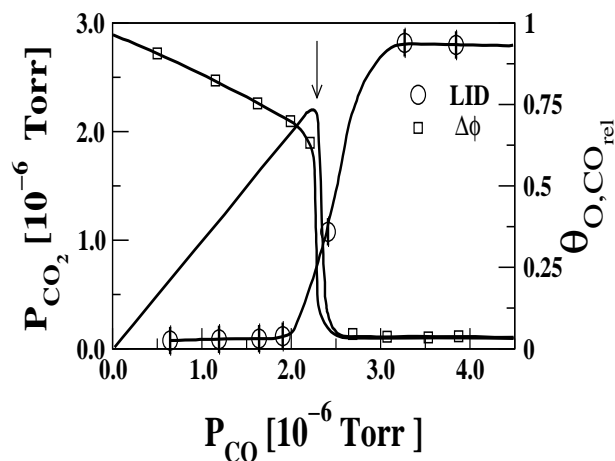


**Figure 2.** Experimental data corresponding to the catalytic oxidation of carbon monoxide on Pt(210) obtained at  $T = 500K$ , keeping the oxygen pressure constant at  $P_O = 2.0 \times 10^{-6}Torr$  and tuning the  $CO$  pressure (horizontal axis). The left vertical axis shows the partial pressure of  $CO_2$  that is proportional to the rate of  $CO_2$  production ( $R_{CO_2}$ ). The right vertical axis shows the surface coverage with  $CO$  ( $\theta_{CO}$ ) and oxygen ( $\theta_O$ ), measured relative to their respective maxima.  $CO$  coverages were measured by means of the absorbate induced work function changes  $\Delta\Phi$ , while oxygen coverages were determined using Laser-Induced Desorption (LID). The transition point is shown with an arrow. Adapted from references [18, 19].

poisoned phase exhibited by the ZGB model within the  $CO$  low-pressure regime is not observed experimentally. Therefore, one lacks experimental evidence of a second-order IPT. ii) The  $CO$ -rich phase exhibiting low reactivity found experimentally resembles the  $CO$ -poisoned state predicted by the ZGB model. However, in the experiments the nonvanishing  $CO$ -desorption probability prevents the system from entering into a truly absorbing state and the abrupt, ‘first-order like’ transition, shown in figure 2 is actually reversible. Of course, these and other disagreements are not surprising since the lattice gas reaction model, with a single parameter, is a simplified approach to the actual catalytic reaction that is far more complex.

At this stage it is worth warning the reader that due to the non-Hamiltonian nature of the ZGB model, as well as all the lattice gas reaction systems that will be treated hereafter, one lacks a thermodynamic quantity, such as the free energy, in order to draw a sharper definition of the order of the transitions. Even more, in contrast to their reversible counterpart, the field of IPT’s lacks a well-established theoretical framework.



Also, it is worth mentioning that systems with absorbing states are clearly out of equilibrium. In fact, the transition rate out of the absorbing state is zero, such as those configurations cannot fulfill standard detailed balance requirements. Therefore, the study of the critical behaviour of these systems must involve IPT's between reactive and absorbing phases. Due to these circumstances, the study of IPT's represents a theoretical challenge within the more general goal of modern physics given by the development of the statistical mechanics of nonequilibrium systems.

It should be recognized that the study of absorbing states and IPT's is almost ignored in the courses of statistical mechanics, in spite of the fact that they abound in physics, chemistry, biology and other disciplines including sociology. Some typical examples include the spreading of epidemics through a population, the propagation of rumors in a society [30], the spreading of fire through a forest [31, 32], coexistence with extinction transitions in prey-predator systems [33] and, of course, catalytic and autocatalytic chemical reactions. From a more general point of view, absorbing states are expected to occur in situations where some quantity of interest can proliferate or die out ( e.g the fire in the forest), without any possibility of spontaneous generation (e.g due to the rays of an electrical storm). The underlying physics involves the competition between proliferation and death of a certain quantity. Proliferation is associated with the active (reactive) phase of the system, while inactivity (poisoning) characterizes the absorbing phase.

## 2. Theoretical Approaches

There are currently three basic approaches for the theoretical modeling of surface reactions: i) *ab-initio* calculations, ii) analytic approaches and iii) stochastic models. The *ab-initio* method is usually implemented via density functional theory approaches and due to the huge computational requirements, the calculations are restricted to few atomic layers of the catalysts and a very reduced catalyst's surface (of the order of  $1nm^2$ ). This approach frequently allows the study of a single adsorbed species or a reactive pair only. Consequently, the study of macroscopic surface systems incorporating statistical effects, as requested for the case of critical phenomena, is impossible at present. So, this approach will not be further discussed here.

On the other hand, stochastic models can account for fluctuations in large systems. So, they are used to deal with a large number of collective phenomena

occurring in reaction systems that are not only restricted to IPT's, but also involve spatio-temporal structures [34, 35], chemical waves [36, 37, 38], kinetic oscillations [39, 40, 41, 42, 43, 44, 45], the transition to chaos [9, 10], etc..

Broad experience gained in the treatment of equilibrium systems has shown that Monte Carlo simulations [27, 28] and Renormalization Group (RG) analysis of classical field-theoretical models [46] are among the most useful tools for the treatment of phase transitions and critical phenomena. A much more reduced experience, obtained during the last decade, indicates that, after some adaptation, similar techniques can also be employed to deal with IPT's.

### *2.1. The Monte Carlo Method*

Monte Carlo (MC) simulations of heterogeneously catalyzed reactions can be considered the computational implementation of microscopic reaction mechanisms. In fact, such mechanisms are the 'rules' of the computer algorithm. Of course, the operation of the rules may lead to the development of correlations, while stochastic fluctuations are inherent to the method.

For the practical implementation of the MC method, the catalyst's surface is replaced by a lattice. Therefore, lattice gas reaction models are actually considered. For this reason, the method often faces the limitations imposed by the size of the lattices used. In some particular cases, e.g. when studying second-order phase transitions, this shortcoming can be overcome appealing to the well-established finite-size-scaling theory [47, 48]. Also, very often one can develop extrapolation methods that give reliable results for the thermodynamic limit, i.e. infinite lattices. Another limitation arises when the diffusion rate of the adsorbed species is very large. In this case, most of the computational time has to be devoted to the diffusion process while the quantity of interest, namely the number of reaction events, becomes negligible. This drawback may be overcome implementing a mixed treatment: mean-field description of the diffusion and MC simulation of the reaction [49, 50]. This approach may become an interesting and powerful tool in the near future.

MC simulations of dynamic and kinetic processes are often hindered by the fact that the Monte Carlo time, usually measured in Monte Carlo time steps, is somewhat proportional to the actual time. So, direct comparison with experiments becomes difficult. However, very recently a more sophisticated implementation of the MC method has been envisioned: namely the Dynamic Monte Carlo (DMC) approach that

incorporates the actual time dependence of the processes allowing direct comparison with experiments [35, 51, 52, 53]. Further developments and applications of the DMC method are a promising field of research.

Within this context, the following subsections describe different MC approaches suitable for the study of IPT's in reaction systems, namely the Standard Ensemble, the Constant Coverage Ensemble and the Epidemic Method. Furthermore, the standard finite-size scaling theory adapted to the case of second-order IPT's and their application to MC data are also discussed.

*2.1.1. The Standard Ensemble* In this ensemble the catalyst is assumed to be in contact with an infinitely large reservoir containing the reactants in the gas phase. Adsorption events are treated stochastically neglecting energetic interactions. The reaction between reactants takes place on the surface of the catalyst, i.e. the so-called Langmuir-Hinshelwood mechanism. After reaction, the product is removed from the surface and its partial pressure in the gas phase is neglected, so that readsorption of the product is not considered.

In order to further illustrate the practical implementation of the Standard Ensemble let us describe the simulation method of the lattice gas reaction version of the catalytic oxidation of  $CO$  (equations (1-3)) according to the ZGB model [26] on the two-dimensional square lattice. The Monte Carlo algorithm is as follows:

i)  $CO$  or  $O_2$  molecules are selected at random with relative probabilities  $P_{CO}$  and  $P_{O_2}$ , respectively. These probabilities are the relative impingement rates of both species, which are proportional to their partial pressures in the gas phase in contact with the catalyst. Due to the normalization,  $P_{CO} + P_{O_2} = 1$ , the model has a single parameter, i.e.  $P_{CO}$ . If the selected species is  $CO$ , one surface site is selected at random, and if that site is vacant,  $CO$  is adsorbed on it according to equation (1). Otherwise, if that site is occupied, the trial ends and a new molecule is selected. If the selected species is  $O_2$ , a pair of nearest-neighbor sites is selected at random and the molecule is adsorbed on them only if they are both vacant, as requested by equation (2).

ii) After each adsorption event, the nearest-neighbors of the added molecule are examined in order to account for the reaction given by equation (3). If more than one  $[CO(a), O(a)]$  pair is identified, a single one is selected at random and removed from the surface.

The phase diagram of the ZGB model, as obtained using the Standard Ensemble,

is shown in figure 1 and will be further discussed in Section 3.1.

*2.1.2. The Constant Coverage Ensemble* Monte Carlo simulations using the Constant Coverage (CC) ensemble, as early proposed by Ziff and Brosilow [54], are likely the most powerful method available for the study of first-order IPT's.

In order to implement the CC method, first a stationary configuration of the system has to be achieved using the Standard Ensemble algorithm, as described in Section 2.1.1. For this purpose, one selects a value of the parameter close to the coexistence point but within the reactive regime. After achieving the stationary state, the simulation is actually switched to the CC method. Then, one has to maintain the coverage with the majority species of the corresponding absorptive state as constant as possible around a prefixed value. This goal is achieved regulating the number of adsorption events of competing species. The ratio between the number of attempts made trying to adsorb a given species and the total number of attempts is the measure of the corresponding effective partial pressure. In this way, in the CC ensemble the coverage assumes the role of the control parameter.

In the case of the ZGB model, the stationary state is usually achieved for  $P_{CO} = 0.51$ . So, in order to maintain the  $CO$  coverage close to the desired value  $\theta_{CO}^{CC}$ , oxygen ( $CO$ ) adsorption attempts take place whenever  $\theta_{CO} > \theta_{CO}^{CC}$  ( $\theta_{CO} < \theta_{CO}^{CC}$ ). Let  $\mathcal{N}_{CO}$  and  $\mathcal{N}_{OX}$  be the number of carbon monoxide and oxygen attempts, respectively. Then, the value of the 'pressure' of  $CO$  in the  $CC$  ensemble ( $P_{CO}^{CC}$ ) is determined just as the ratio  $P_{CO}^{CC} = \frac{\mathcal{N}_{CO}}{\mathcal{N}_{CO} + \mathcal{N}_{OX}}$ . Subsequently, the coverage is increased by small amount, say  $\Delta\theta_{CO}^{CC}$ . A transient period  $\tau_P$  is then disregarded for the proper relaxation of the system to the new  $\theta_{CO}^{CC}$  value, and finally averages of  $P_{CO}^{CC}$  are taken over a certain measurement time  $\tau_M$ .

In the original CC algorithm of Brosilow and Ziff [54] the coverage of  $CO$  was increased stepwise up to a certain maximum value ( $\theta_{CO}^{max}$ ) and the set of points ( $\theta_{CO}^{CC}, P_{CO}^{CC}$ ) were recorded. However, later on it has been suggested [55] that it would be convenient to continue the simulations after reaching  $\theta_{CO}^{max}$  by **decreasing**  $\theta_{CO}^{CC}$  stepwise until  $P_{CO}^{CC}$  reaches a value close to the starting point, namely  $P_{CO}^{CC} = 0.51$ . In fact, this procedure would allow to investigate one possible hysteretic effects at first-order IPT's, which are expected to be relevant as follows from the experience gained studying their counterpart in equilibrium (reversible) conditions.

*2.1.3. Finite-Size Scaling Approach to Second-Order IPT's* Since true phase transitions only occur on the thermodynamic limit and computer simulations are always restricted to finite samples, numerical data are influenced by rounding and shifting effects around pseudo critical points [27, 28]. Within this context the finite-size scaling theory [46, 56] has become a powerful tool for the analysis of numerical results allowing the determination of critical points and the evaluation of critical exponents. All this experience gained in the study of reversible critical phenomena under equilibrium conditions can be employed in the field of second-order IPT's.

In order to perform a finite-size scaling analysis close to a second-order ITP [47, 48] in a reaction system it is convenient to take the concentration of the minority species on the surface,  $(\theta_M)$ , as an order parameter. By analogy to reversible second-order transitions one assumes that

$$\theta_M \propto (P - P_c)^\beta, \quad (5)$$

where  $\beta$  is the order parameter critical exponent and  $P_c$  is the critical value of the control parameter  $P$ . Approaching  $P_c$  from the reactive regime, the characteristic length scale of the system given by the correlation length  $\xi_\perp$  diverges according to

$$\xi_\perp \propto (P - P_c)^{-\nu_\perp}, \quad (6)$$

where  $\nu_\perp$  is the correlation length exponent in the space direction.

For finite samples and close to the critical region, the concentration of minority species will depend on two competing lengths, namely  $\theta_M(L, \xi_\perp)$ , and the scaling hypothesis assumes

$$\theta_M(L, \xi_\perp) = L^{-\beta/\nu_\perp} F[(P - P_c)L^{1/\nu_\perp}], \quad (7)$$

where equation (6) has been used and  $F$  is a suitable scaling function. Just at  $P_c$ , one has

$$\theta_M(L, P_c) \propto L^{-\beta/\nu_\perp}, \quad (8)$$

and

$$F(x) \propto x^\beta, \quad (x \rightarrow \infty), \quad (9)$$

such that equation (5) is recovered when  $L \rightarrow \infty$  in the critical region.

As anticipated by the adopted notation, second-order IPT's exhibit spatio-temporal anisotropy, so that the correlation length in the time direction is given by

$$\xi_{\parallel} \propto (P - P_c)^{-\nu_{\parallel}}, \quad (10)$$

where  $\nu_{\parallel}$  is the corresponding correlation length exponent.

Examples of the application of finite-size scaling to various reaction systems can be found in the literature [47, 48, 57, 58]. However, a more accurate method for the evaluation of critical exponents is to combine finite-size scaling of stationary quantities and dynamic scaling, as will be discussed just below.

*2.1.4. The Epidemic Method and Dynamic Scaling* In order to obtain accurate values of the critical point and the critical exponents using the Standard Ensemble and applying finite-size scaling, it is necessary to perform MC simulations very close to the critical point. However, at criticality and close to it, due to the large fluctuations always present in second-order phase transitions, any finite system will ultimately become irreversibly trapped by the absorbing state. So, the measurements are actually performed within metastable states facing two competing constraints: on the one hand the measurement time has to be long enough in order to allow the system to develop the corresponding correlations and, on the other hand, such time must be short enough to prevent poisoning of the sample. This shortcoming can be somewhat healed by taking averages over many samples and disregarding those that have been trapped by the absorbing state. However, it is difficult to avoid those samples that are just evolving to such absorbing state, unless that fluctuations are suppressed by comparing two different samples evolving through the phase space following very close trajectories [59]. In view of these shortcomings, experience indicates that the best approach to second-order IPT's is to complement finite-size scaling of stationary quantities, as obtained with the Standard Ensemble, with epidemic simulations.

The application of the Epidemic Method (EM) to the study of IPT's has become a useful tool for the evaluation of critical points, dynamic critical exponents and eventually for the identification of universality classes [60, 61, 62]. The idea behind the EM is to initialize the simulation using a configuration very close to the absorbing state. Such a configuration can be achieved generating the absorbing state using the Standard Ensemble and, subsequently, removing some species from the center of the sample where a small patch of empty sites is left. In the case of the ZGB model this can be done by

filling the whole lattice with  $CO$ , except for a small patch. Patches consisting of 3-6 neighboring empty sites are frequently employed, but it is known that the asymptotic results are independent of the size of the initial patch. Such patch is the kernel of the subsequent epidemic.

After the generation of the starting configuration, the time evolution of the system is followed using the Standard Ensemble as already described in Section 2.1.1. During this dynamic process the following quantities are recorded: (i) the average number of empty sites ( $N(t)$ ), (ii) the survival probability  $P(t)$ , which is the probability that the epidemic is still alive at time  $t$ , and (iii) the average mean square distance,  $R^2(t)$ , over which the empty sites have spread. Of course, each single epidemic stops if the sample is trapped in the poisoned state with  $N(t) = 0$  and, since these events may happen after very short times (depending on the patch size), results have to be averaged over many different epidemics. It should be noticed that  $N(t)$  ( $R^2(t)$ ) is averaged over all (surviving) epidemics.

If the epidemic is performed just at critically, a power-law behaviour (scaling invariance) can be assumed and the following ansätze are expected to hold,

$$N(t) \propto t^\eta, \quad (11)$$

$$P(t) \propto t^{-\delta}, \quad (12)$$

and

$$R^2(t) \propto t^z, \quad (13)$$

where  $\eta$ ,  $\delta$  and  $z$  are dynamic critical exponents. Thus, at the critical point log-log plots of  $N(t)$ ,  $P(t)$  and  $R^2(t)$  will asymptotically show a straight line behaviour, while off-critical points will exhibit curvature. This behaviour allows the determination of the critical point and from the slopes of the plots the critical exponents can also be evaluated quite accurately [61].

Using scaling arguments, it has been shown that the following relationship [61]

$$(d+1)z = 4\delta + 2\eta, \quad (14)$$

holds, allowing the evaluation of one exponent as a function of the other two.

The validity of equations (11), (12) and (13) for second-order IPT's is very well established. Furthermore, the observation of a power-law behaviour for second-order IPT's is in agreement with the ideas developed in the study of equilibrium (reversible)

phase transitions: scale invariance reflects the existence of a diverging correlation length at criticality. It should be mentioned that the EM can also be applied to first-order IPT's close to coexistence. However, since it is well known that in the case of first-order reversible transitions correlations decay exponentially, preventing the occurrence of scale invariance, equations (11), (12) and (13) have to be modified. Recently, the following anzats has been proposed [55]

$$N(t) \propto \left(\frac{t}{\tau}\right)^{-\eta^{eff}} \exp\left[-\left(\frac{t}{\tau}\right)\right] \quad (15)$$

where  $\eta^{eff}$  is an effective exponent and  $\tau$  sets a characteristic time scale. So, equation (15) combines a power-law behaviour for  $t \rightarrow 0$  with an exponential (asymptotic) decay.

It should also be mentioned that the whole issue of the occurrence of power-law behaviour at equilibrium first-order transitions is a bit more complex than the simplified arguments used above. For example, scaling behaviour inside the coexistence zone has been observed for the liquid-gas phase transitions using finite systems. However, this scaling disappears on the thermodynamic limit [63]. Also, when a first-order line ends in a second-order critical point, the system frequently displays several decades of critical behaviour (before the exponential roll-off) even when measurements are performed quite a bit beyond the critical point [64].

## 2.2. Analytical Methods

In the field of reversible critical phenomena, the most effective analytical tool for the identification of universality classes is the Renormalization Group analysis of classical field-theoretical models using coarse-grained Ginzburg-Landau-Wilson free-energy functionals [65]. While reaction systems exhibiting IPT's do not have energy functionals, they can often be treated on the coarse-grained level by means of phenomenological Langevin equations. Stochastic partial differential equations of this kind are the natural formalism to analyze critical properties of irreversible systems with absorbing states, as will be discussed below.

On the other hand, Mean-Field modeling using ordinary differential equations (ODE) is a widely used method [14] for the study of first-order IPT's (see also below). Further extensions of the ODE framework, to include diffusional terms are very useful and, have allowed the description of spatio-temporal patterns in diffusion-reaction systems [34]. However, these methods are essentially limited for the study of second-order IPT's because they always consider average environments of reactants and



adsorption sites, ignoring stochastic fluctuations and correlations that naturally emerge in actual systems.

*2.2.1. The Langevin Formulation* The Langevin equation for a single-component field  $\phi(\mathbf{x}, t)$  can be written as [25]

$$\frac{\partial \phi(\mathbf{x}, t)}{\partial t} = F_x(\{\phi\}) + G_x(\{\phi\})\eta(\mathbf{x}, t), \quad (16)$$

where  $F_x$  and  $G_x$  are functionals of  $\phi$ , and  $\eta$  is a Gaussian random variable with zero mean, such that the only nonvanishing correlations are  $\langle \eta(\mathbf{x}, t)\eta(\mathbf{x}', t') \rangle = D\delta(\mathbf{x}-\mathbf{x}')\delta(t-t')$ . Equation (16) is purely first-order in time since it is aimed to describe critical properties where small-wavenumber phenomena dominate the physical behaviour.

The goal of the coarse-grained Langevin representation is to capture the essential physics of microscopic models on large length and time scales. Therefore,  $F_x$  and  $G_x$  are taken to be analytical functions of  $\phi(\mathbf{x}, t)$  and its spatial derivatives. In this way, coarse graining smooths out any nonanalyticity of the underlying microscopic dynamic model.

At this stage, it is clear that one has an infinite number of possible analytical terms in  $\phi$  and its space derivatives that can be placed on the right hand side term of equation (16). Following the ideas of Landau and Lifshitz, it is expected that symmetry considerations would suffice to determine the relevant terms of  $F_x$  and  $G_x$ . In fact, these functional must include all analytic terms consistent with the symmetry of the microscopic model and no term with lower symmetry can be included. The coefficients of these terms are simply taken as unknown parameters or constants to be determined phenomenologically. This assumption is consistent with the fact that the typical IPT's, which are intended to be described with equation (16), can be characterized by a set of critical exponents defining their universality class, which do not depend on the values of the parameters.

Depending on the behaviour of the noise amplitude functional  $G_x$ , two types of physical systems can already be treated:

a) Systems without absorbing states. In this case  $G_x(\phi)$  approaches a constant value. Using Renormalization Group arguments it can be shown that higher powers of  $\phi$  and its derivatives in  $G_x$  are irrelevant for the description of the critical behaviour and therefore, they can be neglected. In this way, the Langevin equation has a simple

additive Gaussian noise of constant amplitude. Assuming that  $F_x(\phi)$  can be written as

$$F_x(\phi) = \Gamma(\nabla^2\phi - r\phi + u\phi^3), \quad (17)$$

where  $r$  and  $u$  are constants, the best known example results in the Ginzburg-Landau-Wilson functional derivative of free energy functional from the Ising model, e.g.

$$\mathcal{H}(\phi) = \int d\mathbf{x}[(\nabla\phi)^2 + r\phi^2/2 + u\phi^4]/4, \quad (18)$$

such that the Langevin equation becomes the celebrated time dependent Ginzburg-Landau equation. This equation is very useful for the treatment of equilibrium critical phenomena and has been quoted here for the sake of completeness only. In fact, in this article, our interest is focused on far-from equilibrium systems, for which  $F_x(\phi)$  cannot be expressed as a functional derivative. Within this context the best known example is the Kardar-Parisi-Zhang (KPZ) equation introduced for the description of the dynamic behaviour of interfaces without overhangs. For systems with interfaces,  $\phi(\mathbf{x}, t)$  is taken as the height at time  $t$  of a site of the interface at position  $\mathbf{x}$ . It has been shown that the functional

$$F_x(\phi) = c\nabla^2\phi + \lambda(\nabla\phi)^2, \quad (19)$$

captures the large scale physics of moving interfaces leading to the KPZ equation [66]

$$\frac{\partial\phi}{\partial t} = c\nabla^2\phi + \lambda(\nabla\phi)^2 + \eta(\mathbf{x}, t). \quad (20)$$

Recent studies have demonstrated that the KPZ equation holds for the treatment of a wide variety of physical situations [67] including the description of the interfacial behaviour of reactants close to coexistence in systems exhibiting first-order IPT's [36, 37], for further details see also Section 3.1.

b) Systems with absorbing states. In the Langevin equations capable of describing these systems, the noise amplitude functional  $G_x(\phi)$  must vanish with  $\phi$  so that the state  $\phi(\mathbf{x}) = 0$  is an absorbing state for any functional  $F_x$  that has no constant piece and therefore it also vanishes with  $\phi$ . It can be demonstrated that  $G_x(\phi) \propto \phi^\alpha$ , for small enough values of  $\phi$ . Also,  $\alpha$  can assume only positive integer and half-odd-integer values. The cases  $\alpha = 1/2$  and  $\alpha = 1$  are those of interest in practice, the former includes the directed percolation (DP) universality class (which is of primary interest in the context of this article because it is suitable for the description of second-order IPT's [68]), while the latter includes the problem of multiplicative noise.

Considering the case of DP [69, 70], one has to keep in mind that the state  $\phi = 0$  must be absorbing, so that both functionals  $F_x(\phi)$  and  $G_x(\phi)$  must vanish as  $\phi \rightarrow 0$ . This constraint implies that terms independent of  $\phi$  must not be considered. Now, imposing the condition of symmetry inversion on the underlying lattice ( $\mathbf{x} \rightarrow -\mathbf{x}$ ), so that terms containing  $\nabla\phi$  are forbidden, the Langevin equation with the lowest allowed terms in  $\phi$  and its derivatives becomes

$$\frac{\partial\phi}{\partial t} = c\nabla^2\phi - r\phi - u\phi^2 + \phi^\alpha\eta(\mathbf{x}, t). \quad (21)$$

where  $c$ ,  $r$  and  $u$  are constants.

Using Renormalization Group methods it can be shown that the critical dimension for equation (21) is  $d_c = 4$  and that the critical exponents in terms of the first order  $\epsilon$ -expansion (here  $\epsilon \equiv 4 - d$ ) are [25]: dynamic exponent  $z^* = 2 - \epsilon/12$ , order parameter critical exponent  $\beta = 1 - \epsilon/6$  and correlation length exponent  $\nu_\perp = (1 + \epsilon/8)/2$ . Also, the scaling relation

$$\beta = \nu_\perp(d - 2 + \eta^*), \quad (22)$$

holds, where  $\eta^*$  is the critical exponent of the two-point correlation function. Therefore, only two of the exponents are truly independent. Notice that equation (22) is a nonequilibrium counterpart of the well-known scaling relation  $2\beta = \nu(d - 2 + \eta)$  valid for a system without absorbing states.

Apart from the scaling relations given by equation (14) and (22), which hold for dynamic and static exponents, the following relationships between exponents have been found to hold [25]:  $2\eta^* = 4 - d - z^*\eta$ ,  $z^* = 2/z$  and  $\delta = \nu_\parallel\beta$ .

It should also be noticed that IPT's subject to extra symmetries, and thus out of the DP universality class, have been identified in recent years. Among them one has systems with symmetric absorbing states [71], models of epidemics with perfect immunization [72, 73], and systems with an infinite number of absorbing states [74, 75]. Additional discussions on these topics are beyond the aim of this article since these situations do not appear in the reaction models discussed here. For further details the reader is addressed to the recent review of Hinrichsen [76].

*2.2.2. Mean-Field Treatments* The Mean Field (MF) approach to irreversible reactions neglects spatial fluctuations and the effect of noise. So, the actual concentrations of the reactants are replaced by averaged values over the sites of the lattice. Differential

equations for the time dependence of such averages are derived for specific reaction systems with different degrees of sophistication, for instance involving one or more site correlations. MF equations are useful in order to get insight into the behaviour of reaction systems close to first-order IPT's where spatial fluctuations are expected to be irrelevant [14].

In spite of the restricted application of MF equations to the study of second-order IPT's, it is instructive to discuss the MF predictions of the Langevin equation (21). In fact, replacing the field  $\phi(\mathbf{x}, t)$  by the spatial constant  $\phi(t)$  and neglecting the noise and the Laplacian terms, equation (21) becomes [25]

$$d\phi/dt = -r\phi - u\phi^2. \quad (23)$$

Equation (23) has two long-time stationary solutions given by the absorbing state ( $\phi = 0$ ) and the active regime ( $\phi = -r/u$ ), which are stable for  $r > 0$  and  $r < 0$ . Here  $r$  plays the role of the control parameter with a critical point at  $r_c = 0$ . The order parameter critical exponent that governs the decay of the average density  $\langle \phi \rangle \approx |r - r_c|^\beta$  for  $r \rightarrow r_c$  from the active phase is  $\beta = 1$ .

### 3. Critical Behaviour of Specific Reaction Systems

The first part of this section will be devoted to describe lattice gas reaction models inspired in actual catalytic reactions, such as the catalytic oxidation of carbon monoxide (Section 3.1) and the reaction between nitric oxide and carbon monoxide (Section 3.2). These models exhibit many features characteristic of first-order IPT's that have also been found in numerous experiments, such as hysteretic effects [17, 77] and abrupt changes of relevant properties when a control parameter is tuned around a coexistence point [17, 18, 19] (see also figure 2), etc. On view of these facts, special attention will be drawn to the discussion of first-order IPT's.

On the other hand, Section 3.3 will be mostly devoted to the discussion of generic models, which are not intended to describe specific reaction systems. Most of these models exhibit second-order IPT's.

#### 3.1. The Catalytic Oxidation of Carbon Monoxide

As already discussed in the introductory sections, the catalytic oxidation of carbon monoxide is one of the most studied reaction due to its practical importance and

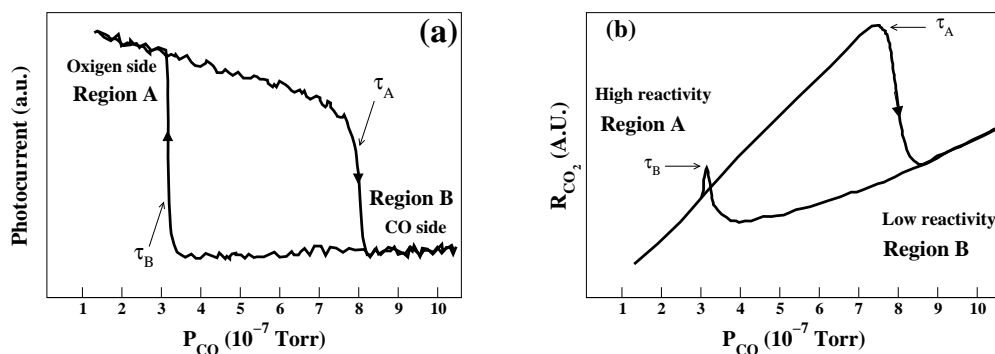


**Figure 3.** Experimental data corresponding to the catalytic oxidation of carbon monoxide on Pt(111) obtained at  $T = 413.2K$ , keeping the oxygen pressure constant at  $P_O = 4.0 \times 10^{-5}Torr$ , while the  $CO$  partial pressure is varied cyclically (horizontal axis). (a) Hysteresis in the reactant coverage as measured by the Photoelectron Emission Microscopy (PEEM) [80] and (b) in the  $CO_2$  reaction rate. More details in the text. Adapted from reference [77].

theoretical interest. The simplest approach for this reaction is the ZGB lattice gas model [26] as described in Section 1 and Section 2.1.1 (for additional details see [12, 15, 16]).

The phase diagram of the ZGB model (figure 1) exhibits a second-order IPT close to  $P_{1CO} \simeq 0.3874$  that belongs to the DP universality class [68]. The dynamic critical exponents, as evaluated using epidemic simulations (Section 2.1.4), equations (11), (12) and (13)), are  $\eta = 0.224 \pm 0.010$ ,  $\delta = 0.452 \pm 0.008$  and  $z = 1.13 \pm 0.01$  (in two dimensions) [60, 78], which, in fact, are in excellent agreement with the accepted exponents of the universality class of the directed percolation, namely  $\eta = 0.2295 \pm 0.0010$ ,  $\delta = 0.44505 \pm 0.0010$  and  $z = 1.1325 \pm 0.0010$  [61, 62, 79]. The order parameter critical exponent, as evaluated using the damage spreading technique [59], is  $\beta = 0.57 \pm 0.01$ , also in excellent agreement with the DP value, namely  $\beta = 0.583 \pm 0.004$  [79].

More interesting, close to  $P_{2CO} = 0.5258$ , the ZGB model exhibits a first-order IPT (see figure 1) in qualitative agreement with experiments performed using single crystal surfaces as catalysts (see figure 2). As mentioned above, the nonvanishing  $CO$  desorption rate experimentally observed [3, 4] prevents the actual catalyst system from entering in to a truly absorbing state and the abrupt transition shown in figure 2 is actually reversible. Further experimental evidence on the existence of this first-order-like behaviour arises from dynamic measurements exhibiting clear hysteretic effects, as shown in figure 3 for the case of the  $CO + O_2$  reaction on a  $Pt(111)$  single crystal surface [77]. Figure 3(a) shows hysteresis in the reactant coverage upon cyclic variation of the  $CO$  partial pressure (horizontal axis). The vertical axis shows the photocurrent measured in a Photoelectron Emission Microscopy (PEEM) [80] experiment. Notice

that a low (negative) photocurrent indicates an oxygen-rich phase (left-hand side of figure 3(a)), while a large photocurrent corresponds to a  $CO$ -rich phase (right-hand side of figure 3(a)). Also, figure 3(b) shows the hysteresis in the rate of  $CO_2$  production (measured using a mass spectrometer) as a function of the  $CO$  partial pressure. When the system is in the low  $CO$  pressure regime, the surface is mostly covered by oxygen that corresponds to the ‘oxygen side’ or monostable region A. Upon increasing  $P_{CO}$  the reaction rate also rises until, close to  $P_{CO} = \tau_A$ , the surface becomes covered with adsorbed  $CO$ . This ‘ $CO$  side’ or monostable state B, corresponds to a low reactivity regime. Decreasing  $P_{CO}$ , the system remains in this monostable region B until, close to  $P_{CO} = \tau_B$ , it suddenly undergoes a steep transition and rapidly returns to the initial state of high reactivity. Summing up, during the hysteresis loop the system may be in two monostable regions A ( $P_{CO} < \tau_B$ ) and B ( $P_{CO} > \tau_A$ ), separated from each other by a bistable region ( $\tau_A > P_{CO} > \tau_B$ ) [77].

In view of this stimulating experimental evidence let us review some numerical studies on hysteretic effects close to coexistence. Figure 4 shows a plot of  $\theta_{CO}$  versus  $P_{CO}$  obtained by means of the  $CC$  ensemble applied to the ZGB model and using a relatively small sample ( $L = 32$ ). Starting from the stationary value of  $\theta_{CO}$  at  $P_{CO} = 0.51$ , one observes that stepwise increments of  $\theta_{CO}$  cause  $P_{CO}$  to increase steadily up to the  $L$ -dependent upper spinodal point  $P_{CO}^S(L = 32) = 0.5330 \pm 0.031$ . Turning around the spinodal point, further increments of  $\theta_{CO}$  cause  $P_{CO}$  to decrease steadily up to  $P_{CO} \approx 0.513$  for  $\theta_{CO}^{max} \approx 0.825$ . At this point the growing  $CO$  branch finishes and the subsequent decrease in  $\theta_{CO}$  causes the system to return to the starting point where the decreasing  $CO$  branch of the loop ends. Notice that both the growing and decreasing branches describe the same trajectory (within error bars) on the  $(\theta_{CO}, P_{CO})$  plane. So, it has been concluded that hysteretic effects are not observed using this small lattice [55].

Increasing the size of the lattice ( $L = 256$  in figure 4(b)), the behaviour of the system changes dramatically. On the one hand, the spinodal point becomes appreciably shifted (see inset of figure 4(b)), and on the other hand, hysteretic effects become evident since  $CO$ -growing and  $CO$ -decreasing branches can be clearly distinguished. Notice that within a remarkably wide range of  $CO$  values both branches are vertical, and consequently parallel each to other. After increasing the lattice size ( $L = 1024$  in figure 4(c)) only minor changes in  $P_{CO}^S$ ,  $P_{CO}^{GB}$ ,  $P_{CO}^{DB}$  occur, but a well defined spinodal point and a hysteresis loop can still be observed (see inset of figure 4(c)).

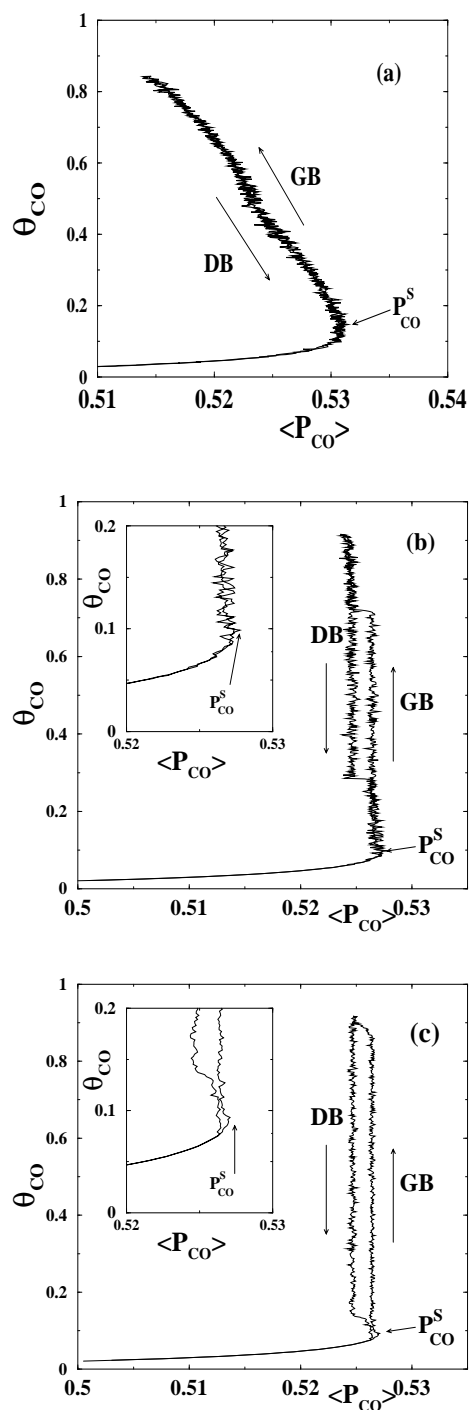


**Figure 4.** Plots of  $\theta_{CO}$  versus  $\langle P_{CO} \rangle$  obtained using the constant coverage ensemble. Results corresponding to  $\tau_P = 100$  mcs,  $\tau_M = 2000$  mcs and a stepwise variation of  $\theta_{CO}$  given by  $\Delta\theta_{CO} = 2 \times 10^{-3}$ . The arrow pointing up (down) shows the growing (decreasing)  $\theta_{CO}$  branches of the loop. The upper spinodal point  $P_{CO}^S$  is also shown; a)  $L = 32$ ; b)  $L = 256$  and c)  $L = 1024$ . The insets of figures (b) and (c) show zooms of the spinodal region.

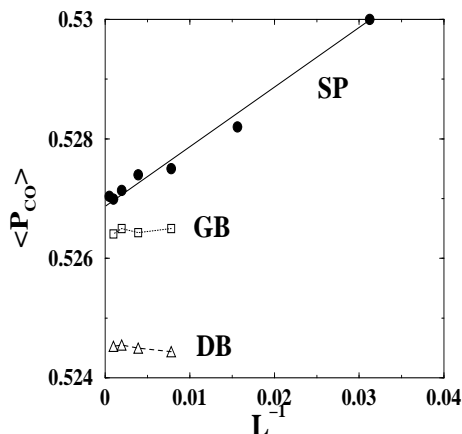


**Figure 5.** Plots of the upper spinodal points determined using lattices of different sizes ( $\bullet P_{CO}^S(L)$ ), the  $CO$  pressure for the growing ( $\square P_{CO}^{GB}$ ), and decreasing branches ( $\triangle P_{CO}^{DB}$ ) versus the inverse lattice size ( $L^{-1}$ ). More details in the text.

Figure 5 shows a plot of the  $L$ -dependent spinodal points ( $P_{CO}^S(L)$ ) versus the inverse lattice size ( $L^{-1}$ ). Performing an extrapolation to the infinite size limit yields  $P_{CO}^S(L = \infty) = 0.5270 \pm 0.0005$  [55]. This figure should be compared with the value reported by Brosilow *et al* [54],  $P_{CO}^S \approx 0.5285$ , which corresponds to a determination of  $P_{CO}^S$  in a finite lattice of size  $L = 1024$ . Also, Evans *et al* [81] have reported  $P_{CO}^S \approx 0.527$  for a finite lattice of size  $L = 256$ . Very recently, an independent estimation given by  $P_{CO}^S = 0.52675 \pm 0.00025$ , which is in excellent agreement with the figures measured using the CC method, has been obtained by means of short-time dynamic measurements [82].

Plots of both  $P_{CO}^{GB}$  and  $P_{CO}^{DB}$  versus  $L^{-1}$ , also shown in figure 5, indicate that finite-size effects are negligible for large lattices ( $L > 512$ ). So, the extrapolated estimates are [55]  $P_{CO}^{GB} \cong 0.5264 \pm 0.0002$  and  $P_{CO}^{DB} \cong 0.52467 \pm 0.0003$ , respectively.

Another interesting feature of  $CC$  simulations showing hysteresis is that one can exchange the role of the axis in the following sense: finely tuning the coverage  $\theta_{CO}$  one can induce the system to undergo first-order transitions in parameter space ( $P_{CO}$  in this case).

Hysteretic effects can be further understood after examination of various snapshot configurations as shown in figure 6. It should be noticed that all of the configurations belong to the coexistence region and, consequently, these states are not allowed when simulating the ZGB model using the standard algorithm since right at  $P_{2CO}$ ,  $\theta_{CO}$  displays a discontinuous jump from  $\theta_{CO} \approx 10^{-3}$  to  $\theta_{CO} = 1$  (see figure 1). Figure 6(a) shows a typical configuration corresponding to the spinodal point  $P_{CO}^S \simeq 0.5270$



with  $\theta_{CO} \cong 0.087$ . Here, one observes that some small but compact  $CO$  clusters have already been nucleated. This configuration is different from those obtained within the reactive regime using the standard algorithm (not shown here for the sake of space) that show mostly  $CO$  monomers with  $\theta_{CO} \approx 10^{-3}$ . The snapshot configurations shown in figures 6(b) and (c) correspond to the growing branch and have been obtained for  $\theta_{CO} \approx 0.30$  and  $\theta_{CO} \approx 0.50$ , respectively. It should be noticed that above  $P_{CO}^S$  a single massive  $CO$  cluster has spread within the reactive phase. In figure 6(b), this massive  $CO$  cluster does not percolate, but increasing  $\theta_{CO}$  percolation along a single direction of the lattice is observed (figure 6(c)). Percolation of the massive cluster along only one direction is observed up to a relatively high  $CO$  coverage ( $\theta_{CO} \cong 0.763$  in figure 6(d)). These values of the  $\theta_{CO}$  are remarkably greater than the percolation threshold of random percolation model, given by  $P_C \approx 0.59275$  [83]. However, the random percolation cluster is a fractal object with fractal dimension  $\mathcal{D}_F \cong 1.89\dots$  [83], while the  $CO$  cluster is a compact object. Dangling ends emerging from the surface of the  $CO$  cluster eventually get in contact causing percolation of such a cluster in both directions of the lattice (figure 6(e)). It should be noticed that the snapshot configuration of figure 6(d) corresponds to the growing branch while that of figure 6(e), which has been taken after few mcs, corresponds to an effective  $CO$  pressure characteristic of the decreasing branch. Therefore, the jump from one branch to the other seems to be accompanied by a change in the configuration of the  $CO$  cluster. It will be interesting to quantitatively study the properties of the interface between the  $CO$  cluster and the reactive phase in order to determine their possible self-affine nature, as well as the interplay between curvature and hysteresis. From the qualitative point of view, the examination of snapshots suggests that both the interface roughness and length of the massive  $CO$  cluster remain almost unchanged for the growing branch. When  $\theta_{CO}$  is further increased, the jump to the decreasing branch is eventually characterized by the onset of percolation along both directions of the lattice and, consequently, the macroscopic length and the curvature of the interface may change. So, the subtle interplay of interfacial properties, such as length, roughness, curvature, etc. has to be studied in detail in order to fully understand the hysteresis loop observed using the  $CC$  ensemble. It is expected that the longer the interface length of the growing branch the easier the  $CO - O$  reaction, so one needs a higher effective  $CO$  pressure to keep the coverage constant. In contrast, along the decreasing branch, the shorter length of the interface inhibits reactions so that a greater oxygen pressure (smaller  $CO$  pressure) is needed to achieve the desired  $CO$  coverage.

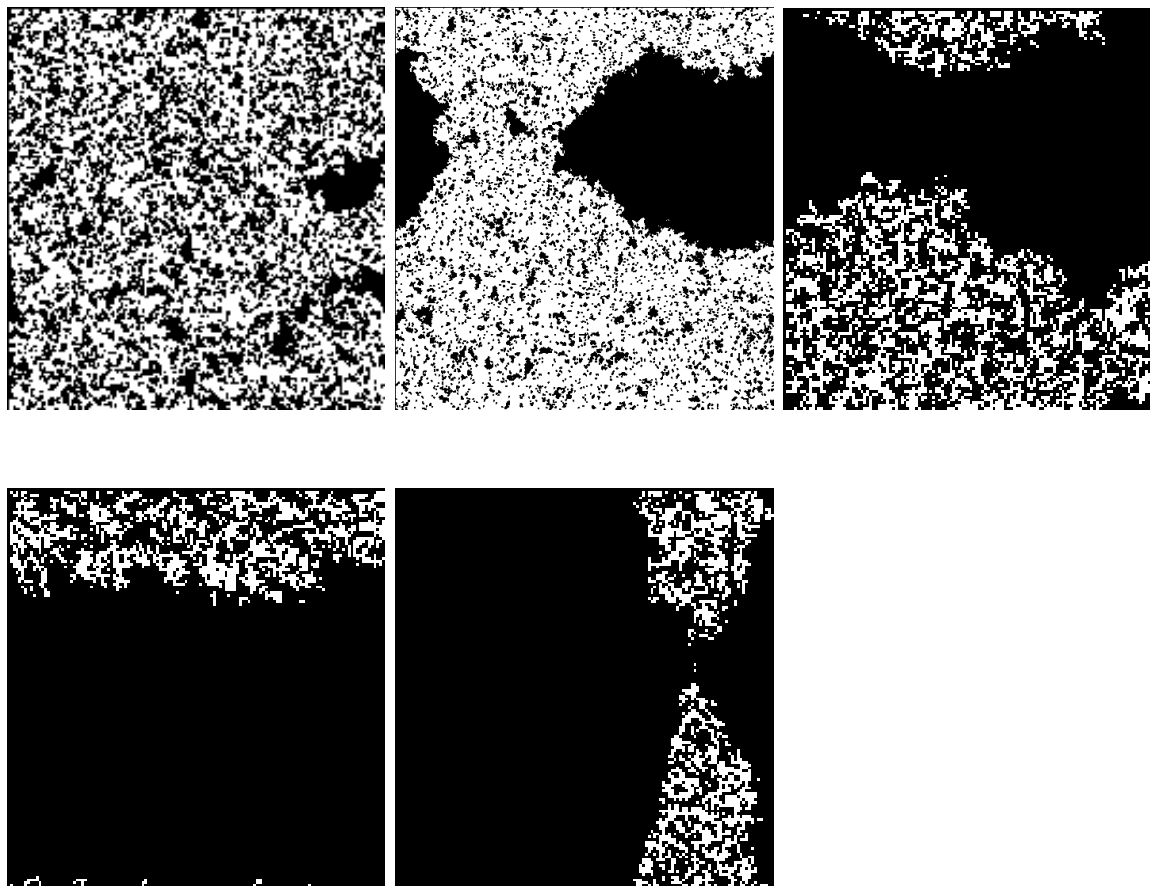


**Figure 6.** Typical snapshot configurations obtained using the constant coverage ensemble and lattices of side  $L = 512$ ,  $CO$ -occupied sites are black while other sites are left white; a) snapshot obtained at the spinodal point with  $\theta_{CO} \approx 0.087$ , b), c) and d) are snapshots obtained along the growing branch with  $\theta_{CO} \approx 0.30$ ,  $\theta_{CO} \approx 0.50$ , and  $\theta_{CO} \approx 0.763$ , respectively; e) snapshot obtained few Monte Carlo steps after figure d) but now the system has jumped to the decreasing branch with  $\theta_{CO} \simeq 0.78$ .

So, these arguments may explain the existence of two branches.

The snapshot configurations of figure 5 unambiguously show the coexistence of two phases, namely a  $CO$ -rich phase dominated by a massive  $CO$  cluster that corresponds to the  $CO$ -poisoned state and a reactive phase decorated with small  $CO$  islands. It should be noticed that such a nice coexistence picture is only available using the  $CC$  ensemble since coexistence configurations are not accessible using the standard ensemble. It should also be noted that the existence of hysteretic effects hinders the location of the coexistence point using the  $CC$  ensemble method. In fact, in the case of hysteresis in thermodynamic equilibrium the chemical potential at coexistence can be obtained after a proper thermodynamic integration of the growing and decreasing branches of the hysteresis loop [84]. For nonequilibrium systems like the ZGB model

where no energetic interactions are considered, the standard methods of equilibrium thermodynamics are not useful. In order to overcome this shortcoming a method based on the spontaneous creation algorithm already used to study different systems [85, 86], has been proposed [55]. The method implies the study of the stability of the hysteresis branches upon the application of a small perturbation. This can be carried out by introducing a negligible small  $CO$  desorption probability ( $P_{CO}^D$ ) to the ZGB model. It is well known that the first-order nature of the IPT of the ZGB model remains if  $P_{CO}^D < 0.1$  [87, 88]. It has been found that taking  $P_D = 10^{-6}$  both branches of the hysteresis loop collapse into a single one that can be identified as the coexistence point given by  $P_{2CO} \cong 0.52583(9)$  [55]. This figure is close to the middle of the hysteresis loop located close to  $P_{2CO} \cong 0.52554 \pm 0.00015$ , where the error bars cover both branches of the loop. The value  $P_{2CO} \approx 0.52560(1)$  reported by Brosilow *et al* [54], which is remarkably close to this figure, has been obtained using the  $CC$  ensemble but neglecting both finite-size and hysteretic effects. Regrettably, the size of the lattice used in reference [54] was not reported, and therefore additional comparisons cannot be performed.

In the seminal paper of Ziff *et al* [26], an estimation of the coexistence point is performed studying the stability of the coexistence phase. This analysis gives  $P_{2CO} \cong 0.525(1)$ , which is also in good agreement with other independent estimates. Also, Evans *et al* [81] have reported  $P_{2CO} = 0.525(1)$  based on the analysis of epidemic simulations. The value reported by Meakin *et al* [89],  $P_{2CO} = 0.5277$ , seems to be influenced by metastabilities due to the large lattices used for the standard simulation method. Therefore, that figure is a bit larger and may correspond to a value close to the spinodal point. Surprisingly, better values, e.g.  $P_{2CO} 0.5255(5)$  [90], can be obtained using very small lattices and the standard algorithm since in such samples metastabilities are short-lived.

Very recently, hysteresis phenomena have been studied on the basis of a modified version of the ZGB model [91]. In fact, it is assumed that the surface of the catalyst has two kinds of inhomogeneities or defects. In type-1 defects, which are randomly distributed on the sample with probability  $p_1$ , the desorption of adsorbed  $CO$  proceeds with probability  $p_{des1}$ . In type-2 inhomogeneities, which are randomly distributed with probability  $p_2$ , the adsorption of oxygen molecules is inhibited and the desorption probability of  $CO$  is given by  $P_{des2}$ . Furthermore,  $p_{des2} < p_{des} < p_{des1}$ , where  $p_{des}$  is the desorption probability of  $CO$  on unperturbed lattice sites. Also, the diffusion of

$CO$  species is considered with probability  $p_{diff}$ , while the probability of other events such as adsorption, desorption and reaction is given by  $p_{chem} = 1 - p_{diff}$ . In order to study hysteric effects the  $CO$  pressure is varied at a constant rate in closed cycles. It is interesting to discuss the mechanisms, which are originated by the definition of the model, which may lead to hysteric effects. In fact, the low desorption probability of  $CO$  prevents the occurrence of a  $CO$  absorbing state and, consequently, the abrupt transition from the high-reactivity state to the low-reactivity regime is reversible. Furthermore, the blocking of lattice sites for oxygen adsorption also prevents the formation of the oxygen-poisoned state and the second-order IPT becomes reversible and takes place between an oxygen-rich low-reactivity regime and a high-reactivity state. Since escaping from both low-reactivity regimes is quite difficult, the occurrence of hysteresis in dynamic measurements can be anticipated.

The reported results obtained by means of simulations [91] (see figure 7) are in qualitative agreement with the experimental findings (figure 3). Figure 7(a) corresponds to the evolution of oxygen coverage.  $\theta_O$  decreases smoothly from the oxygen-rich state when the  $CO$  pressure is raised. This behaviour resembles the case of the ZGB model (figure 1). However, the abrupt increase in  $\theta_O$  observed when  $P_{CO}$  is lowered is due to the fact that the surface is mostly covered by  $CO$  species (see figure 7(b)), which have low desorption probability. In fact, oxygen can only be adsorbed on a nearest-neighbor pair of vacant sites that may become available with (roughly) a low probability of the order of  $(1 - P_{CO})p_{des}^2$ . On the other hand, the growing branch of  $\theta_{CO}$  (figure 7(b)) is flat and that coverage remains close to zero, for  $P_{CO} < 0.48$ . Subsequently, it exhibits an abrupt increase close to  $P_{CO} \simeq 0.5$ , as already expected from the behaviour of the ZGB model (figure 1). The high coverage region of the decreasing branch is due to the low desorption probability of  $CO$  while the subsequent sudden drop is consistent with the abrupt increase in  $\theta_O$  (figure 7(b)). It should be noticed that the experimental measurement of the photocurrent does not allow one to distinguish  $\theta_{CO}$  from  $\theta_O$  [77], so figure 3(a) should be compared with a composition of both figures 7(a) and 7(b). Anyway, the experimental findings are nicely (qualitatively) reproduced by the simulations. Finally, the behaviour of the rate of  $CO_2$  production (figure 7(c)) is also in excellent agreement with the experimental data shown in figure 3(b). As in the experiments [77] (see figure 3), the numerical simulation results shown in figure 7 also allow one to estimate the values of the  $CO$  partial pressure where the transitions from the monostable states A and B to the bistable state,  $\tau_B$  and  $\tau_A$ , respectively take place. Therefore, the width of

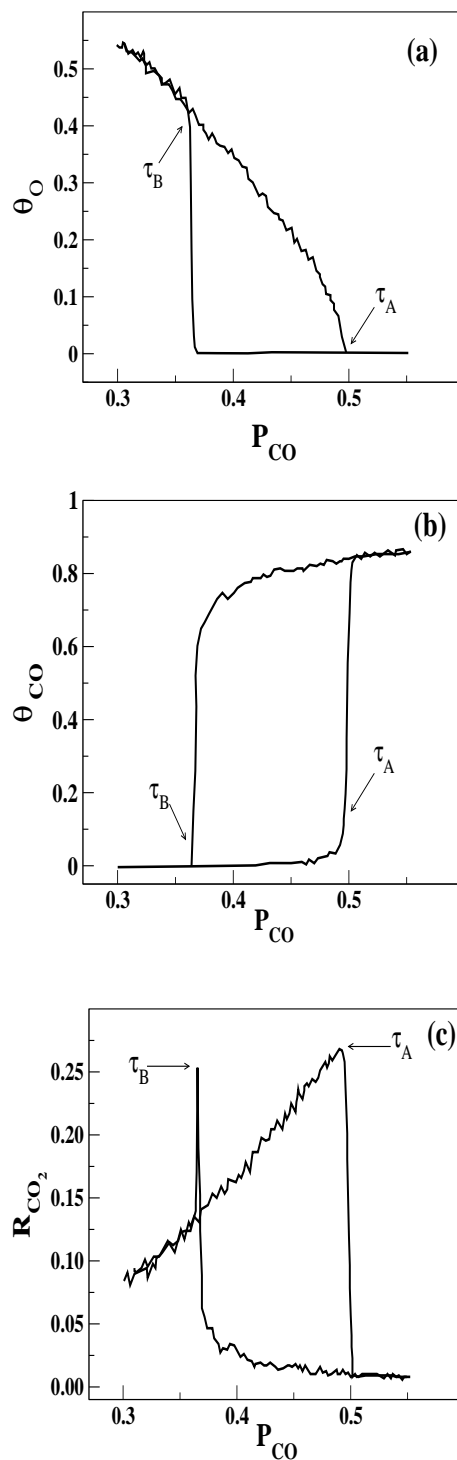


**Figure 7.** Simulation results of hysteresis phenomena obtained using a modified version of the ZGB model, according to Hua and Ma [91]. The simulation parameters are:  $p_{chem} = 0.01$ ,  $p_{des} = 0.1$ ,  $p_{des1} = 0.8$ ,  $p_{des2} = 0.05$ , and  $p_1 = p_2 = 0.1$ . The scanning rate of  $P_{CO}$  is  $\beta_{CO} = \frac{dP_{CO}}{dt} = 0.002/(10mcs)$ . (a) and (b) correspond to the coverages while (c) shows the rate of  $CO_2$  production. More details in the text. Adapted from reference [91].

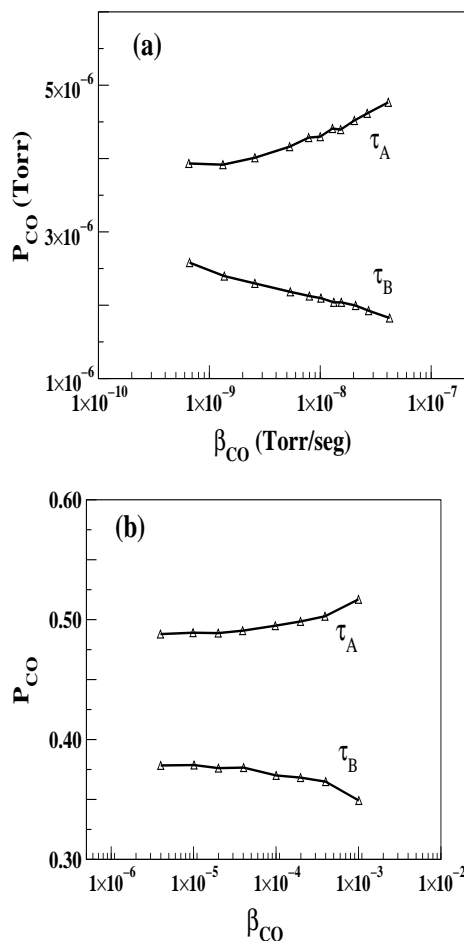


**Figure 8.** Plots of the  $CO$  partial pressure where the transitions from the monostable states A and B to the bistable state,  $\tau_B$  and  $\tau_A$ , respectively take place; versus the scanning rate of  $P_{CO}$  given by  $\beta_{CO} = \frac{dP_{CO}}{dt}$  (a) Experimental data measured under the same conditions as those shown in figure 3. Adapted from reference [77]. (b) Simulation results obtained using the parameters listed in figure 7 but varying the scanning rate of  $P_{CO}$  given in units of  $mcs^{-1}$ . Adapted from reference [91].

the hysteresis loop is given by  $\Delta\tau = \tau_A - \tau_B$ . The dependence of  $\Delta\tau$  on the scan rate of the  $CO$  pressure ( $\beta_{CO} = \frac{dP_{CO}}{dt}$ ) has also been measured experimentally and by means of simulations, as shown in figures 8(a) and 8(b), respectively. Again, the numerical results are in remarkable qualitative agreement with the experiments. Neglecting surface defects and based on mean-field calculations Zhdanov and Kasemo [14] have stated that the two branches of the hysteresis loop should fall together to the equistability point, provided there occurs a sufficiently rapid nucleation and growth of islands. This result is expected to be valid on the limit  $\beta_{CO} \rightarrow 0$  where one also should observe  $\Delta\tau \rightarrow 0$ . As shown in figure 8, the transition points  $\tau_A$  and  $\tau_B$  approach each other and  $\Delta\tau$  shrinks with decreasing  $\beta_{CO}$ . Conclusive evidence on the validity of the mean-field prediction cannot

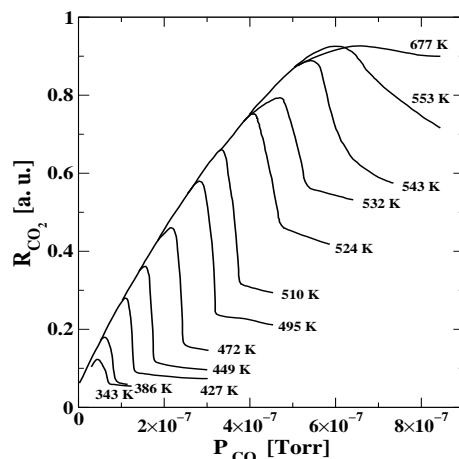


**Figure 9.** Plots of the reaction rate of  $CO_2$  production versus the the partial pressure of  $CO$ . Experiments corresponding to the catalytic oxidation of  $CO$  on  $Pt(111)$  single crystal, performed keeping the oxygen partial pressure constant ( $P_O = 2.0^{-6}$  Torr) and varying the temperature of the catalyst, as shown in the figure. Adapted from references [18, 19].

be found due to either experimental or numerical limitations to achieve a vanishing small scanning rate. However, it has been suggested that  $\delta\tau$  should be finite due to the presence of surface defects [77, 91], which is neglected in the mean-field treatment [14].

Comparing the numerical results obtained applying the CC method to the ZGB model [55] with those of the study performed by Hua *et al* [91], one has to consider that not only both models are different, but also the data corresponding to the CC ensemble were obtained after a long-time stabilization period and consequently exhibit smaller hysteretic effects, in contrast to the dynamic measurements where the relaxation of the system towards stationary states is not allowed [91].

As anticipated above a truly  $CO$ -poisoned state cannot be achieved in the experiments due to the nonvanishing  $CO$ -desorption probability ( $P_{des}^{CO}$ ). According to the theory of thermal desorption and the experiments,  $P_{des}^{CO}$  depends on the temperature of the catalysts and the energetic interactions with neighboring adsorbed species through an Arrhenius factor [92, 93]. Therefore, the magnitude of the abrupt drop in the reaction rate (see figure 2) decreases upon increasing  $T$ , as shown in figure 9 for the case of the catalytic oxidation of  $CO$  on  $Pt(111)$  [18, 19]. Furthermore, on increasing  $T$  the sharp peak of the reaction rate becomes rounded and for high enough temperature, e.g. for  $T \geq 524K$  in figure 8, the signature of the first-order transition vanishes.

The influence of  $CO$  desorption on the phase diagram of the ZGB model has also

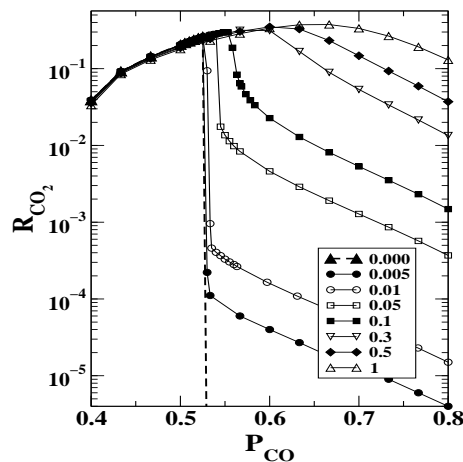


**Figure 10.** Log-linear plots of the reaction rate of  $CO_2$  production versus the the partial pressure of  $CO$ . Results obtained performing Monte Carlo simulations of the ZGB model for different desorption probabilities ( $P_{des}^{CO}$ ), as listed in the figure.

been studied by means of Monte Carlo simulations [87, 88, 91]. The simplest approach is just to introduce an additional parameter to the ZGB model, given by the desorption probability  $P_{des}^{CO}$ . As expected, the second-order IPT of the models is not influenced by  $CO$  desorption [87]. However, the first-order IPT actually disappears because due to the finite value of  $P_{des}^{CO}$  the system can no longer achieve a truly  $CO$ -poisoned state. However, the first-order nature of the transition remains for very low desorption probabilities, as shown in figure 10, for  $P_{des}^{CO} < 0.1$  [87, 88]. On increasing  $P_{des}^{CO}$ , the peak of the rate of  $CO_2$  production becomes shifted and rounded in qualitative agreement with the experiments (figure 9).

Another useful approach to the study of first-order IPT's is to apply the EM as described in section Section 2.1.4. Early epidemic studies of the first-order IPT of the ZGB model have been performed by Evans and Miesch [81]. Epidemic simulations were started with the surface of the catalysts fully covered by  $CO$  species, except for an empty patch placed at the center of the sample. The time dependence of the number of empty sites ( $N(t)$ ) and the survival probability of the patches ( $P(t)$ ) were analyzed in terms of the conventional scaling relationships given by equations (11) and (12). An interesting feature observed in these earlier simulations was the monotonic decrease of  $N(t)$ , which can be fitted with an exponent  $\eta \simeq -2.2$  [81]. This result is in marked contrast with the behaviour expected for second-order IPTs in the DP universality class,



where equation (11) holds with a positive exponent such as  $N(t) \propto t^\eta$  with  $\eta \approx 0.2295$  [78, 79] in two dimensions. Furthermore, it has been observed that empty patches have a extremely low survival probability [81] and the data can be fitted using equation (12) with an exponent  $\delta \simeq 1.97$ , i.e a figure much larger than the exponent expected for DP given by  $\delta \simeq 0.4505$  [78, 79].

Wide experience gained studying **reversible** first-order critical phenomena shows that in this kind of transitions the correlations are short-ranged [94]. Therefore, the reported power-law decays of  $N(t)$  and  $P(t)$  [81] are certainly intriguing. However, recent extensive numerical simulations performed averaging results over  $10^9$  different epidemic runs have changed this scenario [55], as shown in figure 11. In fact, data taken for  $P_{CO}^{GB}$ ,  $P_{2CO}$ , and  $P_{CO}^{DB}$  show pronounced curvature with a clear cut-off, departing from a power-law behaviour as described by equation (11). So, it has been concluded that the occurrence of power law (scale invariance) in the first-order dynamic critical behaviour of the ZGB model can safely be ruled out [55]. On the other hand, for  $P_{CO} \geq P_{CO}^{GB}$ , log-log plots of  $N(t)$  versus  $t$  exhibit pseudo power-law behaviour over many decades ( $10^1 \leq t \leq 10^3$ ), as shown in figure 11. The effective exponent describing the early time behaviour of  $N(t)$  is  $\eta^{eff} \approx -2.0 \pm 0.1$ , in agreement with the result reported by Evans *et al* [81]. However, after a long time, few successful epidemics prevail and the number of empty sites suddenly grows as  $N(t) \propto t^2$ , indicating a spatially homogeneous spreading. The results shown in figure 11 suggest that instead of the power-law behaviour characteristic of second-order transitions (equation (11)), the epidemic behaviour close to first-order IPT's could be described by means of a modified ansatz involving a short-time power-law behaviour followed by a long-time exponential decay, as given by equation (15) [55]. The inset of figure 11 shows a test of equation (15), namely a semilogarithmic plot of  $N(t)(\tau/t)^2$  versus  $t/\tau$ , where  $\eta^{eff} = -2$  has been assumed. The scattering of points for long times is simply due to the reduction of statistics as a consequence of the low survival probability of the initial epidemic patches. Summing up, epidemic studies of the ZGB model close to and at coexistence show a pseudo power-law behaviour for short times ( $t < T$ ) that crosses over to an asymptotic exponential decay for longer times. Consequently, the absence of scale invariance in the first-order IPT of the ZGB model places this kind of transition on the same footing its their reversible counterparts.

Another interesting scenario for the study of bistable behaviour close to first-order IPT's, observed in catalyzed reactions, is to investigate the properties of interfaces

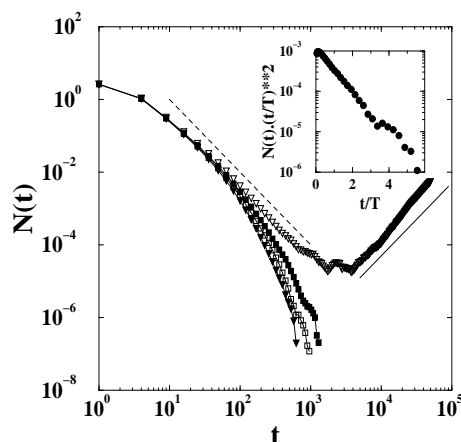


**Figure 11.** Log-Log plots of the number of vacant sites  $N(t)$  versus  $t$  obtained performing epidemic studies of the ZGB model. Results averaged over  $10^9$  different runs ( $\blacktriangledown P_{CO}^{GB}$ ,  $\blacksquare P_{CO}^{DB}$ ,  $\square P_{2CO}$ ,  $\triangledown P_{CO} = 0.52345$ ). For the latter, two straight lines have been drawn for the sake of comparison: the dashed one with slope  $\eta^{eff} = -2$  and the full one with slope 2. The inset shows a semilogarithmic plot of  $N(t)(T/t)^{-2}$  versus  $t/T$  with  $T = 183$ , according to equation (15), obtained at  $P_{2CO}$ . More details in the text.

generated during the propagation of reaction fronts. In fact, key experiments have underlined the importance of front propagation for pattern formation in bistable systems, including the formation of labyrinthine patterns [95], self-replicating spots [96], target patterns and spiral waves [97, 98], stationary concentration patterns (‘Turing structures’) [99], etc. Furthermore, recent experimental studies of catalytic surface reactions have confirmed the existence of a wealth of phenomena related to pattern formation upon front propagation [2, 3, 5, 7, 8, 34, 100].

The basic requirement for the observation of front propagation is a process involving an unstable phase, which could be displaced by a stable one, leading to the formation of an interface where most reaction events take place. This interesting situation is observed close to first-order IPTs, as in the case of the ZGB model (figure 1). In fact, just at the transition point  $P_{2CO}$  one has a discontinuity in  $\theta_{CO}$  that corresponds to the coexistence between a reactive state with small  $CO$  clusters and a  $CO$ -rich phase, which likely is a large  $CO$ -cluster, as suggested by simulations performed using the CC ensemble (see the snapshots of figures 6(b)-(e)). Between  $P_{2CO}$  and the upper-spinodal point  $P_{CO}^{US}$ , the reactive state is unstable and it is displaced by the  $CO$ -rich phase. On the contrary, between the lower spinodal point  $P_{CO}^{LS}$  and  $P_{2CO}$  the reactive state displaces the  $CO$ -rich phase. This latter case has been studied by Evans and Ray [36], who have reported that

the reactive regime displaces the  $CO$ -poisoned state, resulting in a propagation velocity ( $V_p$ ) normal to the interface. It has been proposed that  $V_p$  must vanish as ( $P_{CO} \rightarrow P_{2CO}$ ) [36], where both states become equistable, so one has

$$V_p \propto (P_{CO} - P_{2CO})^{-\gamma}, \quad (24)$$

with  $\gamma > 0$ . The limit of high diffusivity of the reactants can be well described by mean-field reaction-diffusion equations, which give  $\gamma = 1$  [36]. It is interesting to notice that if diffusion is restricted or even suppressed, simulation results give values of  $\gamma$  that are also very close to unity, suggesting that this exponent is independent of the surface diffusivity of the reactants [36].

For an evolving interface, there is a clear distinction between the propagation direction and that perpendicular to it. So it may not be surprising that scaling is different along these two directions. Therefore, an interface lacks self-similarity but, instead, can be regarded as a self-affine object [67]. Based on general scaling arguments it can be shown that the stochastic evolution of a driven interface along a strip of width  $L$  is characterized by long-wavelength fluctuations ( $w(L, t)$ ) that have the following time- and finite-size-behaviour [67]

$$w(L, t) \propto L^\alpha F(t/L^z), \quad (25)$$

where  $F(x) \propto x^{\beta^*}$  for  $x \ll 1$  and  $F(x) \rightarrow 1$  for  $x \gg 1$ , with  $z = \alpha/\beta^*$ . So, the dynamic behaviour of the interface can be described in terms of the exponents  $\alpha$  and  $\beta^*$ , which are the roughness and growth exponents, respectively. Thus, for an infinite system ( $L \rightarrow \infty$ ), one has  $w(t) \propto t^\beta$ , as  $t \rightarrow \infty$ . Note that  $w$  is also known as the interface width.

It is reasonable to expect that the scaling behaviour should still hold after coarse-graining and passing to the continuous limit. In fact, the dynamics of an interface between two phases, one of which is growing into the other, is believed to be correctly described by simple nonlinear Langevin type equations, such as equation (20) proposed by Kardar, Parisi and Zhang (KPZ) [66], the Edward-Wilkinson (EW) equation [101], and others [67].

As in the case of second-order phase transitions, taking into account the values of the dynamic exponents, evolving interfaces can be grouped in sets of few universality classes, such that interfaces characterized by the same exponents belong to the same universality class. Among others, KPZ and EW universality classes are the most frequently found in

both experiments and models [67], including electrochemical deposition, polycrystalline thin-film growth, fire-front propagation, etc. [30, 31, 32, 33].

Pointing again our attention to the simulation results of Evans and Ray [36], they have reported that the propagation of the reaction interface, close to  $P_{2CO}$ , can be described in terms of dynamic scaling arguments [36], with  $\beta^* \simeq 0.3$ , i.e., a figure close to the KPZ value ( $\beta^* = 1/3$  in  $d = 2$  dimensions).

Very recently, Chávez *et al* [102] studied the dynamics of front propagation in the catalytic oxidation of CO on *Pt*(100) by means of a cellular automaton simulation. It is found that the dynamic scaling exponents of the interface are well described by equation (25) with  $\alpha = 1/2$  and  $\beta^* = 1/3$ . It is also reported that, in the absence of surface diffusion, the interface dynamics exhibits KPZ behaviour [102].

Based on a variant of the ZGB model, Goodman *et al* [37] have studied the propagation of concentration waves. They reported the observation of trigger waves within the bistable regime of the process, i.e., close to the first-order IPT. In fact, within this regime one has the coexistence of a stable state with a metastable one. At the boundary between the two, the stable state will displace the metastable one and the boundary will move, so this process leads to the propagation of concentration fronts (trigger waves). Goodman *et al* [37] found that the velocity of the *CO* front depends on the diffusion rate  $D_{CO}$  of *CO* species (diffusion of oxygen is neglected) and ( $P_{CO}$ ). The velocity of the front vanishes on approaching the poisoning transition at  $P_{2CO}(D_{CO})$  (note that the transition point now depends on  $D_{CO}$ ), according to equation (24), with  $\gamma \simeq 1$ , in agreement with the results of Evans *et al* [36].

While front propagation during the catalytic oxidation of *CO* on platinum surfaces has been observed in numerous experiments [2, 8, 3, 5, 100], the quantitative analysis of data is somewhat restricted by the fact that the fronts are neither flat nor uniformly curved, eventually several of them nucleate almost at the same time and, in most cases, the occurrence of strong interactions between fronts ('interference of chemical waves') makes clean interpretations quite difficult. In order to overcome these shortcomings, Haas *et al* [7] have studied the propagation of reaction fronts on narrow channels with typical widths of 7, 14 and 28  $\mu m$ . The main advantage of these controlled quasi-one-dimensional geometries is that frequently only a single front propagates along the channel, thus avoiding front interactions. Additionally, the narrowness of the channels and the absence of undesired flux at the boundaries lead to practically planar fronts. Using this experimental setup, the front velocity in different channels can be measured

as a function of the partial pressure of  $CO$ , keeping the temperature and the oxygen partial pressure constant, as shown in figure 12(a). At low  $P_{CO}$  values only oxygen fronts are observed. Furthermore, their velocity decreases when  $P_{CO}$  is increased, reaching a minimum value at a certain critical threshold  $P_{CO}^{crit2}$  (see figure 12(a)). When  $P_{CO}$  is further increased a jump is observed- now the front reverses itself into a  $CO$  front and travels in the opposite direction. When  $P_{CO}$  is lowered from high values, the  $CO$  fronts become slower and hysteresis is observed (see the coexistence between Oxygen and  $CO$  fronts in figure 12(a) for  $P_{CO} < P_{CO}^{crit2}$ ). Finally, at  $P_{CO}^{crit1}$  another jump is observed- under these conditions  $CO$  fronts can no longer persist below a quite low (but nonzero velocity) and they reverse themselves into fast Oxygen fronts (figure 12(a)). Many features of the experiment of Haas *et al* [7] can be recovered simulating front propagation with the aid of the ZGB model on the square lattice with rectangular geometries of sides  $L \times M$  ( $L \ll M$ ) [38]. Thus  $L$  is the width of the channel and  $M$  its length. Free boundary conditions were taken along the channel while the opposite ends are assumed to be in contact with oxygen and  $CO$  sources, respectively. If  $O$  or  $CO$  species are removed from the ends of the channels (i.e., the ‘sources’), due to the reaction process, they are immediately replaced. The propagation of the  $CO$  concentration profile was studied starting with a sample fully covered by oxygen, except for the first and second columns, which are covered by  $CO$  (the  $CO$  source), and left empty, respectively. The propagation of the oxygen profile was followed using a similar procedure [38]. Under these conditions one always has two competing interfaces along the channel.

In order to make a quantitative description of the propagation, the concentration profiles of the reactants,  $\theta_O(x)$  and  $\theta_{CO}(x)$ , are measured along the length of the channel  $x$  in the  $M$ -direction and averaged over each column of lattice sites of length  $L$ . Then, the moments of the profiles, which in subsequent steps can be used to determine the propagation velocity and the width of the profiles, are also measured. In fact, the moments of  $n$ th order of the profiles can be evaluated according to [103]

$$\langle x^n \rangle_{\theta} = \frac{\sum x^n [\theta(x+1) - \theta(x)]}{\sum [\theta(x+1) - \theta(x)]}. \quad (26)$$

Thus, using equation (26) the velocity of propagation can be obtained from the first moment

$$V = \frac{d \langle x \rangle}{dt}. \quad (27)$$

Monte Carlo simulation results show that the front propagation velocity depends on both  $P_{CO}$  and the channel width  $L$ , as shown in figure 12(b). This figure also

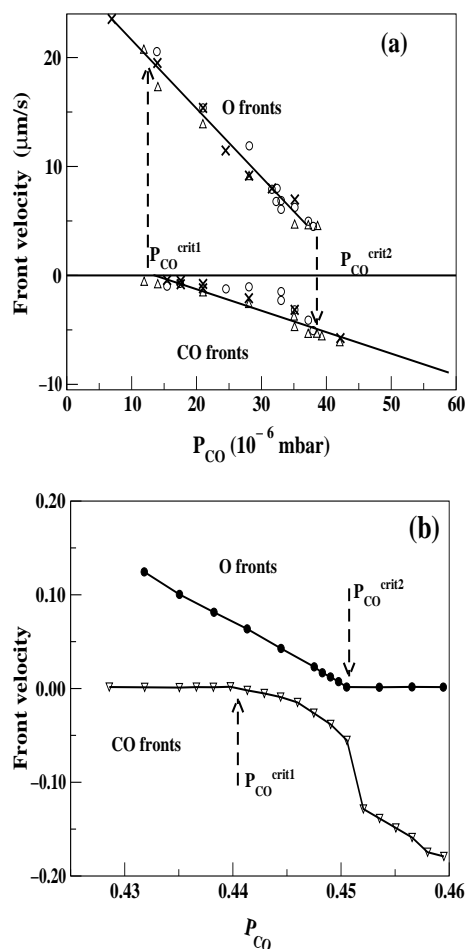


**Figure 12.** (a) Experimental results showing the front velocity inside three channels (triangles:  $28\mu\text{m}$ , circles  $14\mu\text{m}$ , and crosses  $7\mu\text{m}$ ) as a function of  $\text{CO}$  partial pressure. Data measured taking  $P_{\text{O}} = 4 \times 10^{-4}$  mbar and  $T = 360$  K. More details in the text. Adapted from reference [7]. (b) Monte Carlo results obtained with the ZGB model for front propagation in channels of  $L = 10$  lattice units (LU). Plots of the front velocity (in units of LU per mcs) versus  $\text{CO}$  partial pressure. The lines show the critical pressures at which propagation stops. Adapted from reference [38].

shows that the displacement of  $\text{CO}$ - and  $\text{O}$ -poisoned channels by the reactive regime stops at certain ( $L$ -dependent) critical values,  $P_{\text{CO}}^{c2}(L)$  and  $P_{\text{CO}}^{c1}(L)$ , respectively. By means of an extrapolation to the thermodynamic limit it is possible to identify these critical values with the critical points of the ZGB model, namely  $P_{\text{CO}}^{c1}(L \rightarrow \infty) = P_{1\text{CO}}$  and  $P_{\text{CO}}^{c2}(L \rightarrow \infty) = P_{2\text{CO}}$ , respectively. It is also found that close to  $P_{\text{CO}}^{c2}$ , when the propagation of the  $\text{O}$  profile ceases, the velocity of the  $\text{CO}$  profile undergoes a sharp change. This behaviour can be correlated with the first-order IPT between the stationary reactive regime and the  $\text{CO}$ -poisoned state observed in the ZGB model at  $P_{2\text{CO}}$  (see figure 1).

So far, the main conclusions that can be drawn from figure 12(b) can be summarized as follows: a) there are two critical pressures,  $P_{CO}^{c1}(L)$  and  $P_{CO}^{c2}(L)$ , which depend on the width of the channel, at which propagation of one profile or the other stops; b) within these critical values, propagating  $CO$  and  $O$  profiles coexist; c)  $O$  profiles propagate faster than  $CO$  profiles. All these observations appear in qualitative agreement with the experimental results shown in figure 12(a) [7]. However, the underlying physics is different: in the simulations the displacement of a poisoned phase by the invading reactive phase takes place within a range of pressures where the latter is unstable, while the former is stable. In contrast, the experiment may show the propagation of coexisting phases within a bistable regime [7].

So far, all those simulations of the ZGB model discussed above do not attempt to describe the occurrence of oscillations in the concentration of the reactants and in the rate of production, which are well documented by numerous experiments [3, 5, 18, 19]. In fact, it is well known that the catalytic oxidation of  $CO$  on certain  $Pt$  surfaces exhibits oscillatory behaviour, within a restricted range of pressures and temperatures, which is associated with adsorbate-induced surface phase transitions [3, 5]. Since the aim of this paper is to describe the irreversible critical behaviour of the reaction, the oscillatory behaviour will not be further discussed. Therefore, the interested reader is addressed to recent developments involving the study of numerous lattice-gas models aimed to explain the oscillations observed experimentally [35, 41, 42, 43, 44, 45, 104].

Since the ZGB lattice gas reaction model is an oversimplified approach to the actual processes involved in the catalytic oxidation of  $CO$ , several attempts have been made in order to give a more realistic description. Some of the additional mechanisms and modifications added to the original model are the following: (i) The inclusion of  $CO$  desorption [18, 19, 105, 106, 107] that causes the first-order IPT to become reversible and slightly rounded, in qualitative agreement with experiments (figures 9 and 10). (ii) Energetic interactions between reactants adsorbed on the catalyst surface have been considered by various authors [105, 108, 109]. In general, due to these interactions the IPT's become shifted, rounded and occasionally they are no longer observed [105, 108, 109, 110]. (iii) Studies on the influence of the fractal nature of the catalyst are motivated by the fact that the surface of most solids at the molecular level must be considered as a microscopic fractal, such as the case of catalysts made by tiny fractal metallic cluster dispersed in a fractal support or in a discontinuous thin metal films. The fractal surfaces have been modeled by means of random fractals,

such as percolating clusters, [111, 112, 113], diffusion limited aggregates [114] and also deterministic fractals, such as Sierpinsky carpets, [115, 116], etc. [117, 118]. One of the main findings of all these studies is that the first-order IPT becomes of second-order for dimensions  $D_F < 2$ . Since in  $d = 1$  dimensions the ZGB model does not exhibit a reaction window, one may expect the existence of a ‘critical’ lower fractal dimension capable a sustaining a reactive regime. This kind of study, of theoretical interest in the field of critical phenomena, remains to be addressed. (iv) Also, different kinds of adsorption mechanisms, such as hot-dimer adsorption [119], local versus random adsorption [120, 121], nonthermal mechanisms involving the precursor adsorption and diffusion of  $CO$  molecules [122], the presence of subsurface oxygen [123], etc. have been investigated. (v) The influence of surface diffusion has also been addressed using different approaches [105, 124, 125, 126]. Particularly interesting is the hybrid lattice-gas mean-field treatment developed by Evans *et al* [50] for the study of surface reactions with coexisting immobile and highly mobile reactants. (vi) Considering the Eley-Rideal mechanism [127, 128] as an additional step of the set of equations (1-3), namely including the following path



poisoning of the surface by complete occupation by  $O$  species is no longer possible preventing the observation of the second-order IPT. (vii) The influencia of surface defects, which has also been studied, merits a more detailed discussion because, in recent years, considerable attention has been drawn to studies of surface reactions on substrates that include defects or some degrees of geometric heterogeneity, which is not described by any fractal structure, as in the case of item iii). Interest in these types of substrates is based on the fact that the experiments have shown that inert species capable to block adsorption sites, such a sulfur, deposit on the catalyst surface during the exhaust of the combustion gases. Also crystal defects that are formed during the production of the catalyst result in blocked sites. Other inhomogeneities consist of crystallographic perturbations but may equally well involve active foreign surface atoms. Recently Lorenz *et al* [129] have performed Monte Carlo simulations using three different types of defective sites. Site-1, that adsorbed neither  $O$  nor  $CO$  and Site-2 (Site-3) that adsorbed  $O$  ( $CO$ ) but no  $CO$  ( $O$ ). They found that  $CO$  islands form around each defect near  $P_{2CO}$  ( $P_{CO} = 0.524 - 0.526$ ). The average density of  $CO$  decays as a power-law of the radial distance from the defect ( $\rho_{CO} = kr^{-m}$ ,  $m = 1.90(2)$ ), and the average cluster



size also obeys a power-law with the distance to spinodal point ( $\Delta P = P_{CO}^S - P_{CO}$ ) with exponent 0.73. When defects are randomly distributed, with density  $\theta_d$ ,  $P_{2CO}$  decreases linearly according to  $P_{2CO} = -0.307\theta_d + 0.5261$ . This model has also been investigated in the site and pair mean-field approximations [130]. The pair approximation exhibits the same behaviour that the Monte Carlo simulation. The size of the reactive windows decreases with  $\theta_d$  and the abrupt transition at  $P_{2CO}$  becomes continuous (the same behaviour have been reported in a related model [131]). However, unlike the analytical results, in the Monte Carlo simulation there is a critical concentration above which the transition at  $P_{2CO}$  becomes continuous ( $\theta_d = 0.75$  in agreement with previous results [132]). In conclusion, various models shown that the presence of defects on the catalytic surface causes the  $CO$  poisoning transition to occur at lower  $P_{CO}$  values than on homogeneous surfaces. Also, beyond some critical concentration of defects, the first-order IPT of the ZGB model becomes second-order. The overall effect of inert sites is to reduce the production of  $CO_2$ . Furthermore, these findings provide an alternative explanation for the absence of a second-order IPT into a  $O$ -poisoned state observed in the experiments of  $CO$  oxidation (see figure 2).

### 3.2. The Catalytic Reaction Between Nitrogen Monoxide and Carbon Monoxide.

The catalytic reduction of  $NO$  with various agents, including  $CO$ ,  $H_2$ ,  $NH_3$ , hydrocarbons, etc., has been extensively studied on  $Pt$  and  $Rh$  surfaces [3, 5], which are the noble metals used in automotive catalytic converters, due to the key role played by  $NO_x$  emission in air pollution [133]. Aside from the practical importance, the catalytic reduction of  $NO$  also exhibits a rich variety of dynamic phenomena including multistability and oscillatory behaviour [3, 5]. Within this context, the catalytic reaction between  $NO$  and  $CO$  is the subject of this section.

The archetypal model used in most simulations has early been proposed by Yaldran and Khan (YK) [134]. As in the case of the ZGB model [26], the YK model is also a lattice gas reaction system based on the Langmuir-Hinshelwood mechanism. The reaction steps are as follows





where  $S$  represents an unoccupied site on the catalyst surface,  $2S$  represents a nearest neighbor (NN) pair of such sites,  $(g)$  indicates a molecule in the gas phase and  $(a)$  indicates an species adsorbed on the catalyst. The reactions given by equations (31) and (32) are assumed to be instantaneous (infinity reaction rate limit) while the limiting steps are the adsorption events given by equations (29) and (30). The YK model is similar to the ZGB model for the  $CO + O_2$  reaction, except that the  $O_2$  is replaced by  $NO$ , and NN  $N$  atoms, as well as NN  $CO - O$  pairs, react. For further details on the YK model see [134, 135, 136, 137, 138, 139].

Early simulations of the YK model have shown [134, 135] that a reactive window is observed on the hexagonal lattice while such kind of window is absent on the square lattice [134, 135], pointing out the relevance of the coordination number for the reactivity. Therefore, we will first discuss Monte Carlo simulations of the YK model performed on the hexagonal (triangular) lattice. Subsequently, results obtained for variants of the YK model that also exhibit reaction windows on the square lattice will be presented.

The simulation procedure in the standard ensemble is as follows: let  $P_{NO}$  and  $P_{CO}$  be the relative impingement rates for  $NO$  and  $CO$ , respectively, which are taken to be proportional to their partial pressures in the gas phase. Taking  $P_{CO} + P_{NO} = 1$ , such normalization implies that the YK model has a single parameter that is usually taken to be  $P_{CO}$ .  $CO$  and  $NO$  adsorption events are selected at random with probabilities  $P_{CO}$  and  $1 - P_{CO}$ , respectively. Subsequently, an empty site of the lattice is also selected at random. If the selected species is  $CO$ , the adsorption on the empty site occurs according to equation (30). If the selected molecule is  $NO$ , a NN site of the previously selected one is also chosen at random, and if such site is empty the adsorption event takes place according to equation (29). Of course, if the NN chosen site is occupied the adsorption trial is rejected. After each successful adsorption event all NN sites of the adsorbed species are checked at random for the occurrence of the reaction events described by equations (31) and (32).

During the simulations, the coverages with  $CO$ ,  $O$  and  $N$  ( $\theta_{CO}$ ,  $\theta_O$  and  $\theta_N$ , respectively) as well as the rate of production of  $CO_2$  and  $N_2$  ( $R_{CO_2}$ ,  $R_{N_2}$ , respectively) are measured. The phase diagram of the YK model, shown in figure 13, is similar to that of the ZGB model [26] shown in figure 1. In fact, in both cases second- and first-

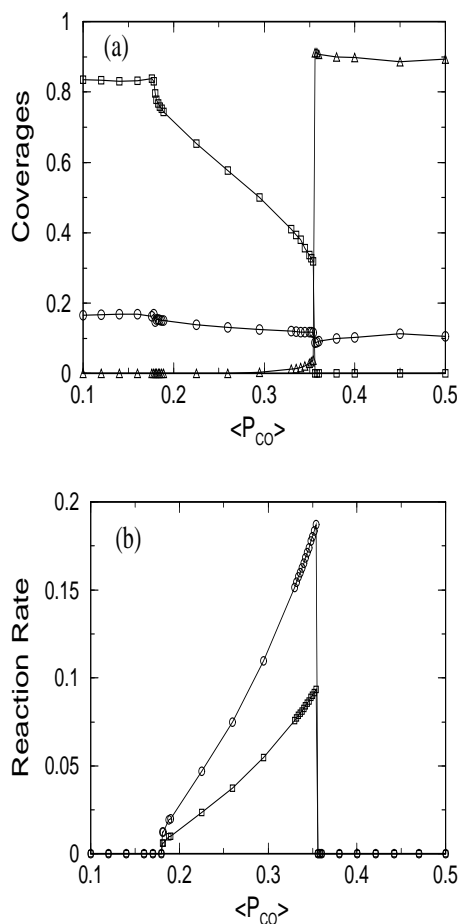


**Figure 13.** Phase diagram of the YK model on the hexagonal lattice of size  $L=128$ . (a) Plots of  $\theta_{CO}(\Delta)$ ,  $\theta_O(\square)$  and  $\theta_N(\circ)$  versus  $\langle P_{CO} \rangle$ . (b) Plots of  $R_{N_2}(\square)$  and  $R_{CO_2}(\circ)$ ; measured as units of number of  $N_2$  and  $CO_2$  molecules removed from the lattice per unit area and time, respectively; versus  $\langle P_{CO} \rangle$ .

order IPT's are observed. However, in contrast to the ZGB model where the absorbing (poisoned) states are unique, in the case of the YK model such states are mixtures of  $O(a) + N(a)$  and  $CO(a) + N(a)$  as follows from the observation of the left and right sides of the phase diagram, respectively (figure 13(a)). The IPT observed close to  $P_{1CO} = 0.185 \pm 0.005$  [134, 135, 139] is continuous and therefore of second-order (see figure 13). More interesting, an abrupt first-order IPT is also observed close to  $P_{2CO} = 0.3545 \pm 0.005$  (figure 1(a) and (b)) [134, 135, 139].

Hysteretic effects close to the first-order IPT of the YK model have been investigated using the CC ensemble [139] (see Section 3.2). For small lattices ( $L \leq 64$ ) the relaxation time is quite short, so that hysteretic effects are absent. This result is in agreement with similar measurements of the ZGB model (see figure 4(a)). On

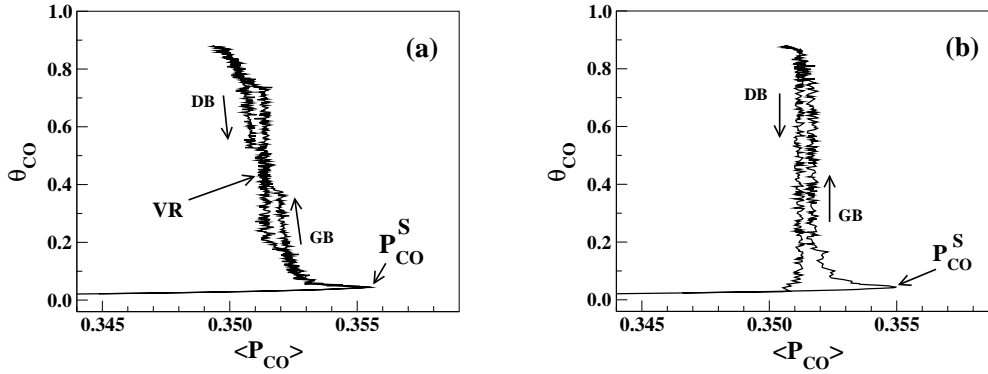


**Figure 14.** Plots of  $\theta_{CO}$  versus  $\langle P_{CO} \rangle$  obtained using the CC ensemble and taking: (a)  $L = 256$  and (b)  $L = 1024$ . The arrows indicate the growing branch (GB), the decreasing branch (DB), the vertical region (VR) and the upper spinodal point ( $P_{CO}^S$ ). More details in the text.

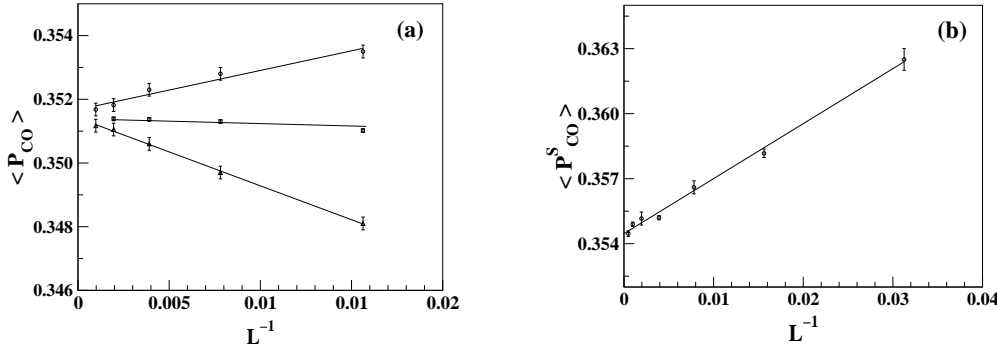


**Figure 15.** (a) Plots of  $\langle P_{CO} \rangle$  versus  $L^{-1}$  measured in the growing branch ( $\circ$ ), decreasing branch ( $\triangle$ ), and the vertical region ( $\square$ ). The straight lines correspond to the best fits of the data that extrapolate to  $L \rightarrow \infty$ . (b) Plots of  $P_{CO}^S$  versus  $L^{-1}$ . The straight line corresponds to the best fit of the data that extrapolates to  $P_{CO}^{US}(L \rightarrow \infty) = 0.3544(2)$ . More details in the text.

increasing the lattice size, hysteretic effects can be observed even for  $L \geq 128$  and they can unambiguously be identified for  $L = 256$ , as shown in figure 14(a). A vertical region located at the center of the loop and slightly above  $\langle P_{CO} \rangle \approx 0.35$ , as well as the upper spinodal point  $P_{CO}^{US}$ , can easily be observed in figure 14. Furthermore, it is found that while the location of  $P_{CO}^{US}$  is shifted systematically toward lower values when  $L$  is increased, the location of the vertical region (close to the center of the loops) remains almost fixed very close to  $P_{CO} = 0.3515$  [139]. Using lattices of size  $L = 1024$ , the hysteretic effects are quite evident (see figure 14(b)) and also, the growing and decreasing branches of the loops are almost vertical. Also, the location of these branches depends on the lattice size, as follows from the comparison of figures 14(a) and (b). A more quantitative analysis on the behaviour of  $P_{CO}$  corresponding to the different branches and the vertical region has also been reported [139]. Figure 15(a) shows the

dependence of the location of the growing branch and the decreasing branch ( $P_{CO}^{GB}$  and  $P_{CO}^{DB}$ , respectively) on the inverse of the lattice size. The  $L$  dependence of  $P_{CO}$  at the vertical region ( $P_{CO}^{VR}$ ) is also shown for the sake of comparison. It has been found that the location of all relevant points, namely  $P_{CO}^X$  with  $X = GB, DB$  and  $VR$ , depends on the curvature radius ( $s$ ) of the interface of the massive  $CO$  cluster in contact with the reactive region. Such dependence can be written as follows

$$P_{CO}^X = P_{CO}^X(L \rightarrow \infty) + F^X(s), \quad (33)$$

where  $P_{CO}^X(L \rightarrow \infty)$  is the location of the point under consideration after proper extrapolation to the thermodynamic limit and  $F(s)$  is an  $s$ -dependent function. For the vertical region one has  $s \rightarrow \infty$  and  $P_{CO}^{VR}$  is almost independent of  $L$ , so  $F^{VR}(\infty) \rightarrow 0$ , as shown in figure 15(a). In contrast, for the DB and the GB,  $s$  is finite and of the order of  $-1/L$  and  $1/L$ , respectively. So, one has  $F^{DB}(s) \approx -A/L$  while  $F^{GB}(s) \approx B/L$ , in agreement with the results shown in figure 15(a). The extrapolated points are

$$P_{CO}^{GB}(L \rightarrow \infty) = 0.3514(3), P_{CO}^{DB}(L \rightarrow \infty) = 0.3517(3) \text{ and } P_{CO}^{VR}(L \rightarrow \infty) = 0.35145(5)$$

Also,  $A \approx 0.215(5)$  and  $B, \approx 0.12(2)$  have been [139].

On the basis of these results,  $P_{CO}^{VR}(L \rightarrow \infty)$  has been identified as the coexistence point  $P_{CO}^{Coex} \cong 0.35145(5)$  in excellent agreement with an independent measurement,  $P_{2CO} = 0.35140 \pm 0.00001$ , reported by Brosilow and Ziff [135]. This result is in contrast with measurements performed with the ZGB model. In fact, for the ZGB systems the vertical region is not observed while the locations of the growing and decreasing branches are almost independent of the lattice size (see figure 4). The explanation of the difference observed comparing both models, which may be due to the different behaviour of the interface of the massive  $CO$  cluster, is an interesting open question.

It has also been reported that the location of the upper spinodal point depends on the lattice size, as shown in figure 15(b). This dependence of  $P_{CO}^{US}(L)$  is due to local fluctuations in the  $CO$  coverage that take place during the nucleation of the critical cluster [139]. The extrapolation of the data shown in figure 15(b) gives  $P_{CO}^{US}(L \rightarrow \infty) \cong 0.3544(2)$ . Furthermore, the coverage at this point is  $\theta_{CO}^{US} \cong 0.043(1)$ . These results point out that in the thermodynamic limit the spinodal point is very close to coexistence, i.e.,  $\Delta P_{CO} = P_{CO}^{US} - P_{CO}^{Coex} \cong 0.003$ . For the sake of comparison it is worth mentioning that for the ZGB model one has  $\Delta P_{CO} \cong 0.0012$  (see Section 3.1).

Further insight into the first-order IPT of the YK model can be gained performing epidemic studies. However, in this case it is necessary to account for the fact that the

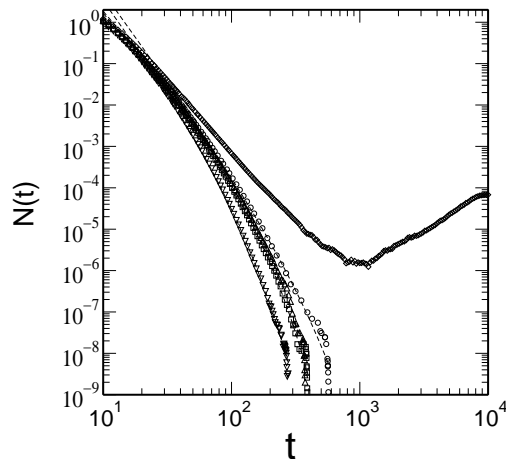


**Figure 16.** Log-log plots of the number of vacant sites  $N(t)$  versus  $t$  obtained performing epidemic simulations using lattices of size  $L = 256$ . Results averaged up to  $3 \times 10^9$  different runs ( $\nabla P_{CO}^S = 0.3544$ ,  $\square P_{CO}^{GB} = 0.3522$ ,  $\triangle P_{CO}^{Coex} = 0.35145$ ,  $\circ P_{CO}^{DB} = 0.3506$  and  $\diamond P_{CO} = 0.3470$ ).

poisoned (absorbing) state above coexistence is nonunique, since it is due to a mixture of  $CO$  and  $N$  atoms with coverage  $\theta_{CO} \approx 0.9$  and  $\theta_N \approx 0.1$ , as shown in figure 13(a). So, the starting configuration has to be obtained running the actual dynamics of the system slightly above coexistence until ‘natural’ absorbing states suitable for the studies are generated.

Figure 16 shows results obtained performing epidemic simulations for various values of  $P_{CO}$  including  $P_{CO}^{Coex}$ ,  $P_{CO}^{US}$ ,  $P_{CO}^{DB}$ ,  $P_{CO}^{GB}$  as well as a value close to coexistence but slightly inside the active region, namely  $P_{CO} = 0.347$ . From figure 16, it becomes evident that the method is quite sensitive to tiny changes of  $P_{CO}$ . The obtained curves are fitted by equation (15) with  $\eta_{eff} = -4.0 \pm 0.5$ , indicating a markedly low survivability of the epidemic patches as compared with the ZGB model that gives  $\eta_{eff} = -2.0 \pm 0.1$ , as already discussed in Section 3.1. The main finding obtained using epidemic studies is that the occurrence of a power-law scaling behaviour close to coexistence can unambiguously be ruled out. This result is in qualitative agreement with data of the ZGB model, see Section 3.1. All these observations are also in agreement with the experience gained studying first-order reversible phase transitions where it is well established that correlations are short ranged, preventing the emergence of scale invariance.

It should be mentioned that several mean-field theories of the YK model have been proposed [135, 136, 138, 140]. Truncating the hierarchy of equations governing the cluster probabilities at the 1-site level, a reasonable estimate of the coexistence

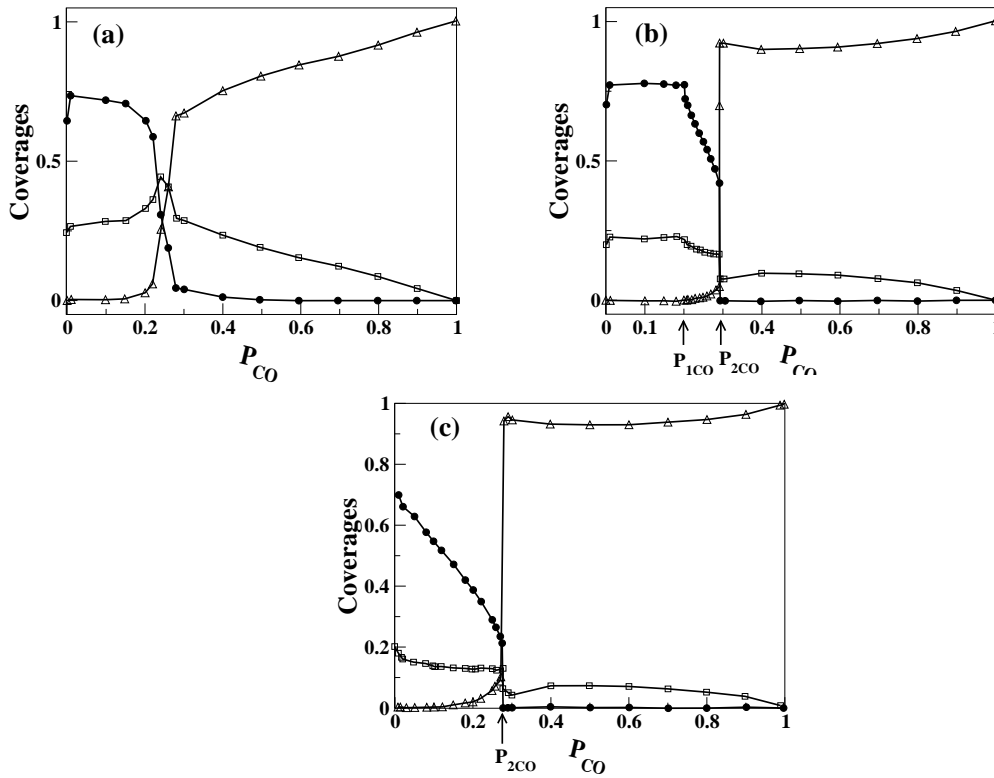
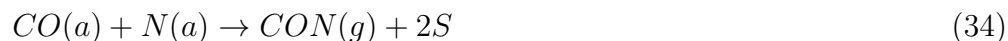


**Figure 17.** Monte Carlo simulation results of the YK model on the square lattice showing plots of species coverages versus  $P_{CO}$ .  $\theta_O$  (empty triangles),  $\theta_N$  (empty squares), and  $\theta_{CO}$  (solid circles). (a) Results obtained neglecting  $N$  diffusion showing the absence of a reaction window such that the catalyst always remains poisoned by mixtures of adsorbed species. (b) Results obtained considering  $N$  diffusion. In this case the YK model exhibits a reaction window. Adapted from reference [141]. (c) Results obtained considering the influence of the Eley-Rideal (ER) mechanism and the diffusion on  $N$ . Adapted from reference [142]. More details in the text.

point given by  $P_{2CO} = 0.3877$  is obtained [135, 136] on the triangular lattice. However, this approach fails to predict the second-order IPT observed in the simulations (see figure 13) [135, 136]. Also, Kortlüke *et al* [140] have derived an accurate prediction of the second-order critical point at  $P_{1CO} = 0.152$  using a two-site cluster approximation. The prediction of this approach for the coexistence point is less satisfactory, namely  $P_{2CO} = 0.393$ . On the other hand, very recently an elaborated mean-field theory of the YK model has been developed up to the pair-approximation level [138] that yields a very accurate estimation of the coexistence point, namely  $P_{2CO} = 0.363$ .

As already mentioned above, the behaviour of the YK model on the square lattice is radically different than that observed on the triangular lattice. In fact, in the former **no** reactive stationary state has been observed [134, 135], as shown in figure 17(a). However, simulation results have shown that diffusion of  $N$  (but not of  $O$ , or  $CO$ ) restores the

possibility of a reactive state [140, 141], as shown in figure 17(b). In fact, in this case a second-order IPT is observed close to  $P_{1CO} = 0.203 \pm 0.001$ , while a first-order IPT is found at  $P_{2CO} = 0.293 \pm 0.001$  [141]. Also, Meng *et al* [137] have shown that by adding a new reaction channel to YK model (equations (29-32)), such that



the reactivity of the system becomes enhanced and consequently a reaction window is observed on the square lattice. This window exhibits a second-order IPT close to  $P_{1CO} = 0.262$  and a first-order IPT close to  $P_{2CO} = 0.501$ . This behaviour is reminiscent of that observed modeling the ZGB model, as discussed above.

On the other hand, assuming that the dissociation of  $NO$  given by equation (29) is preceded by a molecular adsorption on a single site, namely



and



the YK model also exhibits a reaction window in the square lattice provided that both  $NO$  and  $CO$  desorption are considered [137].

Very recently, Khan *et al* [142] have studied the influence of the Eley-Rideal (ER) mechanism (reaction of  $CO$  molecules with already chemisorbed oxygen atoms to produce desorbing  $CO_2$ ) on the YK model on the square lattice. In the absence of  $N$  diffusion, the added ER mechanism causes the onset of a reactive regime at extremely low  $CO$  pressures, i.e., for  $P_{CO} \leq 0.03$ . However, considering the diffusion of  $N$  species, the window becomes considerably wider and the reactive regime is observed up to  $P_{2CO} \simeq 0.29$  where a first-order IPT is found [142], as shown in figure 17(c). This finding suggests that the incorporation of the ER mechanisms does not affect the first-order IPT (see figure 17(b)). In contrast, the second-order IPT is no longer observed as shown in figure 17(c).

As in the case of the ZGB model, the bistable behaviour of the YK model close to coexistence provides the conditions for the displacement of reactive fronts or chemical waves. Within this context, Tammaro and Evans [143] have studied the reactive removal of unstable mixed  $CO + NO$  layers adsorbed on the lattice. Furthermore, in order to account for the diffusion of the reactants, the hopping of all adsorbed species (except for  $O$  atoms whose mobility is negligible) has been considered. Simulations are started



with the surface fully covered by a mixture  $CO + NO$ . This mixture is unstable since the vacation of a single site may produce the dissociation of  $NO$  (equation (36)) and its subsequent reaction with  $CO$  followed by desorption of the products and the generation of empty sites capable of triggering the autocatalytic reaction. Due to the high mobility of most adsorbed species, initially an exponential increase in the number of highly dispersed vacancies is observed. Thereafter, a reaction front forms and propagates across the surface at constant velocity [143]. It is also interesting to remark that all simulation results are confirmed by an elaborated mean-field treatment of chemical diffusion on mixed layers, incorporating its coverage-dependent and tensorial nature, both of these features reflecting the interference of chemical diffusion of adsorbed species on surface by coadsorbed species [143].

### 3.3. Brief Overview of Other Surface Reaction Processes

In addition to the ZGB and the YK models, numerous lattice gas reaction models have also been proposed attempting to describe catalyzed reaction processes of practical and academic interest. Among others, the dimer-dimer (DD) surface reaction scheme of the type  $\frac{1}{2}O_2 + H_2 \rightarrow H_2O$  has been proposed in order to describe the catalytic oxidation of hydrogen [74]. Monte Carlo simulations of the DD model have shown the existence of second-order IPT's and a rich variety of irreversible critical behaviour [74, 144, 145, 146, 147, 148, 149]. Relevant numerical results have also been qualitatively reproduced by mean-field calculations [145].

On the other hand, the catalytic synthesis of ammonia from hydrogen and nitrogen on iron surfaces ( $N_2 + 3H_2 \rightarrow 2NH_3$ ) is among the catalyzed reactions of major economical importance. Ever since its discovery and technical realization, the reaction has become the focus of fundamental investigations. Very recently, various lattice gas reaction models have been proposed and studied by means of numerical simulations [150, 151]. The existence of IPT's has been observed, as shown in figure 18 for the case of the model proposed by Khan and Ahmad (KA) [150]. Here the Langmuir-Hinshelwood reaction mechanism is assumed and the control parameter is the partial pressure of  $H_2$ . As follows from figure 18, the KA model exhibits a second-order (first-order) IPT close to  $P_{1H_2} \simeq 0.445$  ( $P_{2H_2} \simeq 0.585$ ), resembling the behaviour of both the ZGB and the YK models (see figures 1 and 13, respectively).

Recently, the simulation of reaction processes involving more than two reactants has received growing attention. One example of these processes is a multiple-reaction surface

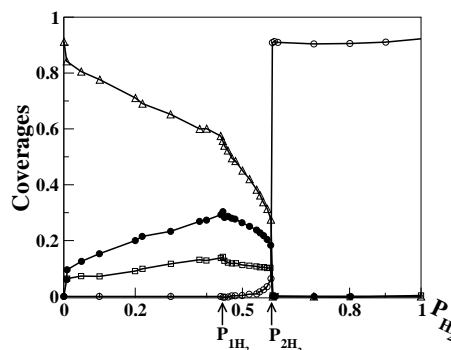


**Figure 18.** Monte Carlo simulation results of the KA model on the square lattice showing plots of species coverages versus  $P_{H_2}$ .  $\theta_H$  (open circles),  $\theta_N$  (empty triangle)  $\theta_{NH}$  (open squares) and  $\theta_{NH_2}$  (solid circles). Adapted from reference [150].

reaction model based upon both the ZGB and the DD models [152, 153, 154]. So, this ZGB-DD model may be applied to the oxidation of CO in the presence of  $H_2$ -traces as well as to the oxidation of hydrogen in the presence of CO-traces. Interest on this model is due to various reasons. For example, the oxidation of hydrogen and carbon monoxide plays a key role in the understanding of the process of hydrocarbon oxidation. In fact, the oxy-hydrogen reaction mechanism contains the chain-branching steps producing O, H and OH-radicals that attack hydrocarbon species. Also, CO is the primary product of hydrocarbon oxidation and it is converted to carbon dioxide in a subsequent slow secondary reaction. Furthermore, the ZGB-DD model exhibits interesting irreversible critical behaviour with nonunique multi-component poisoned states [152, 153, 154].

There are also models that are not aimed to describe any specific reaction system but, instead, they are intended to mimic generic reactions. Typical examples are the monomer-monomer model [26], the dimer-trimer model [155, 156, 157], the monomer-trimer model [158], etc. (see also references [12, 15, 16]).

On the other hand, in the literature there is a vast variety of lattice gas reaction models following the spirit of the reaction described in the above subsections. They all exhibit the same type of irreversible critical behaviour at the transition, which is determined by a common feature- the existence of an absorbing or poisoned state, i.e., a configuration that the system can reach but from where it cannot escape anymore, as discussed in detail in Section 1.2. As already discussed, the essential physics for the occurrence of IPT's is the competition between proliferation and death of a relevant quantity. So, it is not surprising that a large number of models satisfying this condition, and aimed to describe quite diverse physical situations, have been proposed and studied.

Some examples of models exhibiting second-order IPT's are, among others 'directed percolation' as a model for the systematic dripping of a fluid through a lattice with randomly occupied bonds [12, 69, 70], the 'contact process' as a simple lattice model for the spreading of an epidemics [12, 13, 159, 160], 'autocatalytic reaction-diffusion models' aimed to describe the production of some chemical species [161], 'the stochastic game of life' as a model for a society of individuals [162, 163], 'forest fire models' [31, 32], 'branching annihilating random walkers' with odd number of offsprings [58, 164, 165], epidemic spreading without immunization [72], prey-predator systems [33], the Domany-Kinzel cellular automata [166], etc. For an excellent review on this subject see [76].

The common feature among all these models is that they exhibit second-order IPT's belonging to the universality class of directed percolation (DP), the Langevin equation (Section 2.2.1) being the corresponding field-theoretical representation. The robustness of these DP models with respect to changes in the microscopic dynamic rules is likely their most interesting property. Such robustness has led Janssen and Grassberger [167, 168] to propose the so-called DP conjecture, stating that models in the DP universality class must satisfy the following conditions: (i) They must undergo a second-order IPT from a fluctuating active state to a unique absorbing state. (ii) The transition has to be characterized by a positive single-component order parameter. (iii) Only short-range processes are allowed in the formulation of the microscopic dynamic rules. (iv) The system has neither additional symmetries nor quenched randomness. In spite of the fact that the DP conjecture has not been proved rigorously, there is compelling numerical evidence supporting it [169].

So far, DP appears to be the generic universality class for IPT's into absorbing states, having a status similar to their equilibrium counterpart, namely the venerated Ising model. However, despite the successful theoretical description of the DP process, there are still no experiments where the critical behaviour of DP has been observed. Therefore, this is a crucial open problem in the field of IPT's. For further discussions see for instance [170].

#### 4. Conclusions

The study of irreversible critical behaviour in reaction systems has attracted the attention of many physicists and physical-chemists for more than four decades. On the one hand, second-order IPT's are quite appealing since, like the archetypal case of

DP, they are observed in simple models in terms of their dynamic rules. Nevertheless, second-order behaviour is highly nontrivial and has not yet been solved exactly, even using minimal models in one dimension. Furthermore, the critical exponents are not yet known exactly. Field-theoretical calculations and numerical simulations have greatly contributed to the understanding of second-order irreversible behaviour. Most systems lie in the universality class of DP, which plays the role of a standard universality class similar to the Ising model in equilibrium statistical physics, and the reason for few of the exceptions found are very well understood. The main challenges in the field are, from the theoretical point of view, the achievement of exact solutions even for simple models and, from the point of view of the experimentalists, the realization of key experiments unambiguously showing DP behaviour.

On the other hand, the scenario for the state of the art in the study of first-order IPT's is quite different. Firstly, there is stimulating experimental evidence of the existence of abrupt (almost irreversible) transitions, while hysteretic effects and bistable behaviour resembling first-order like behaviour have been observed in numerous catalyzed reaction experiments. Secondly, one still lacks a theoretical framework capable describing first-order IPT's and theoretical efforts are being addressed to the development of mean-field approaches with different degrees of sophistication.

The achievement of a theoretical framework enabling the treatment of irreversible critical behaviour and the gathering of further experimental evidence, including the accurate measurement of critical exponents, are topics of high priority that will certainly contribute to the development of a general theory of the physics of far-from equilibrium processes.

### **Acknowledgments**

This work is financially supported by CONICET, UNLP and ANPCyT (Argentina). We are grateful with numerous colleagues for stimulating discussions.

## 5. References

- [1] Hilderbrand M, Kuperman M, Wio H, Mikhailov A and Ertl G 1999 *Phys. Rev. Lett.* **83** 1475
- [2] Rose K, Berton B, Imbihl R, Engel W and Bradshaw A 1997 *Phys. Rev. Lett.* **79** 3427
- [3] Imbihl R 1993 *Prog. Surf. Sci.* **44** 185
- [4] Ertl G 1990 *Adv. Catal.* **37** 213
- [5] Imbihl R and Ertl G 1995 *Chem. Rev.* **95** 697
- [6] Hopkinson A, Bradley J M, Guo X-C and King D A 1993 *Phys. Rev. Lett.* **71** 1597
- [7] Haas G, Bar M, Kevrekides I G, Rasmussen P B, Petermund H H and Ertl G 1995 *Phys. Rev. Lett.* **75** 3560
- [8] Jabubith S, Rotermund H H, Engel W, von Oertzen A and Ertl G 1990 *Phys. Rev. Lett.* **65** 3013
- [9] Fichthorn K, Gulari E and Ziff R M, 1989 *Phys. Rev. Lett.* **63** 1527
- [10] Fichthorn K, Gulari E and Ziff R M 1989 *Chem. Eng. Sci.* **44** 1403
- [11] Suchorski Y, Beben J, James E, Evans J W and Imbihl R 1999 *Phys. Rev. Lett.* **82** 1907
- [12] Marro J and Dickman R 1999 *Nonequilibrium Phase Transitions and Critical Phenomena* (Cambridge: Cambridge University Press)
- [13] Liggett T M 1985 *Interacting particle systems* (New York: Springer-Verlag)
- [14] Zhdanov V P and Kasemo B 1994 *Surf. Sci. Report* **20** 111
- [15] Albano E V 1996 *Heter. Chem. Rev* **3** 389
- [16] Albano E V 2000 *Computational methods in Surface and Colloid Science* ed Borówko M (New York : Marcel Dekker Inc) p 387
- [17] Christmann K 1991 *Introduction to Surface Physical Chemistry* (Darmstadt: Steinkopff Verlag) p 1
- [18] Ehsasi M, Matloch M, Franck O, Block J H, Christmann K, Rys F S and Hirschwald W 1989 *J. Chem. Phys.* **91** 4949
- [19] Block J H, Ehsasi M and Gorodetskii V 1993 *Prog. Surf. Sci.* **42** 143
- [20] Wintterlin J, Volkening S, Janssens T, Zambelli T, and Ertl G 1997 *Science* **278** 1931
- [21] Hla S-W Bartels L Meyer G and Rieder K-H 2000 *Phys. Rev. Lett.* **85** 2777
- [22] Hendriksen B L M and Frenken J W M 2002 *Phys. Rev. Lett.* **89** 046101
- [23] Engel T and Ertl G 1978 *J. Chem. Phys.* **69** 1267
- [24] Engel T 1978 *J. Chem. Phys.* **69** 373
- [25] Grinstein G and Muñoz M A 1997 *Fourth Granada Lectures in Computational Physics* ed Garrido P L and Marro J (Berlin: Springer) p 223
- [26] Ziff R M, Gulari E, and Barshad Y 1986 *Phys. Rev. Lett.* **56** 2553
- [27] Binder K 1997 *Rep. Prog. Phys.* **60** 487
- [28] Binder K and Heermann D 2002 *Monte Carlo simulations in Statistical Physics. An Introduction* Fourth Ed (Berlin: Springer)
- [29] Meakin P and Scalapino D J 1987 *J. Chem. Phys.* **87** 731
- [30] Zanette D 2002 *Phys. Rev. E* **65** 041908
- [31] Clar S, Drossel B and Schwabl F 1996 *J. Phys. C.: Condens. Matter.* **8** 6803
- [32] Albano E V 1994 *J. Phys. A: Math. Gen.* **27** L881
- [33] Rozenfeld A F and Albano E V 2001 *Phys. Rev. E* **63** 061907
- [34] Walgraef D 1997 *Spatio-temporal pattern Formation* (New York: Springer Verlag)
- [35] Gelten R J, Jansen A P J and van Santen R A 1998 *J. Chem. Phys.* **108** 5921
- [36] Evans J W and Ray T R 1994 *Phys. Rev. E* **50** 4302
- [37] Goodman R H, Graff D S, Sander L M, Leroux-Hugon P and Clément E 1995 *Phys. Rev. E.* **52** 5904
- [38] Albano E V 1997 *Phys. Rev. E.* **55** 7144
- [39] Vigil R D and Willmore F T 1996 *Phys. Rev. E* **54** 1225
- [40] Jansen A P J and Nieminen R M 1997 *J. Chem. Phys.* **106** 2038
- [41] Sander L M and Ghaisas S V 1997 *Surf. Sci.* **391** 125

- [42] Albano E V 1997 *Langmuir* **13** 4013
- [43] Albano E V 1998 *Phys. Rev. E* **57** 6840
- [44] Albano E V 1998 *J. Chem. Phys.* **109** 7498
- [45] Kusovkov V N, Kortluke O and von Niessen W 1998 *J. Chem. Phys.* **108** 5571
- [46] Cardy J 1997 *Scaling and Renormalization in Statistical Physics* Ed Goddard P and Yeomas J M (Cambridge: Cambridge University Press)
- [47] Albano E V 1990 *Phys. Rev. B* **42** R10818
- [48] Aukrust T, Browne D A and Webman I 1990 *Phys. Rev. A* **41** 5294
- [49] Silverberg M and Ben-Shaul A 1987 *J. Chem. Phys.* **87** 3178
- [50] Tammaro M Sabella M and Evans J W 1995 *J. Chem. Phys.* **103** 10277
- [51] Fichtorn K A and Weinberg W H 1991 *J. Chem. Phys.* **95** 1090
- [52] Meng B and Weinberg W H 1994 *J. Chem. Phys.* **100** 5280
- [53] Jansen A P J 1995 *Comp. Phys. Commun.* **86** 1
- [54] Ziff R M and Brosilow B J 1992 *Phys. Rev. A* **46** 4630
- [55] Monetti R and Albano E V 2001 *J. Phys. A: Math. Gen.* **34** 1103
- [56] Barber M N 1983 *Phase transitions and Critical Phenomena* vol II, ed Domb C and Lewobitz J L (London: Academic Press) p 146
- [57] Jensen I and Dickman R 1993 *Phys. Rev. E* **48** 1710
- [58] Jensen I 1994 *Phys. Rev. E* **50** 3623
- [59] Albano E V 1994 *Phys. Rev. E* **49** 1738
- [60] Jensen I, Fogedby H, and Dickman R 1990 *Phys. Rev. A* **41** R3411
- [61] Grassberger P and de la Torre A 1979 *Ann. Phys. (New York)* **122** 373
- [62] Grassberger P, 1989 *J. Phys. A: Math. Gen.* **22** 3673
- [63] Gulminelli F and Comaz P 1999 *Phys. Rev. Lett.* **82** 1402
- [64] Perković O, Dahmen K and Sethna J P, *Phys. Rev. Lett.* **75** 4528
- [65] Binney J J, Dowrick N J, Fisher A J and Newman M E J 1993 *Theory of Critical Phenomena, An Introduction to the Renormalization Group* (Oxford: Clarendon Press)
- [66] Kardar M, Parisi G and Zhang Y C 1986 *Phys. Rev. Lett.* **56** 889
- [67] Barabási A L and Stanley H E 1995 *Fractal Concepts in Surface Growth* (Cambridge: Cambridge University Press)
- [68] Grinstein G, Lai Z-W and Browne D A. 1989 *Phys. Rev. A* **40** 4820
- [69] Broadbent S R and Hammersley J M 1957 *Proc. Camb. Philos. Soc.* **53** 629
- [70] Deutscher G, Zallen R and Adler J (ed) 1980 *Annals of the Israeli Physical Society* vol 5 (Bristol: Hilger)
- [71] Cardy J L and Täuber U C 1996 *Phys. Rev. Lett.* **70** 4780
- [72] Grassberger P 1982 *Math. Biosci.* **63**, 157
- [73] Janssen H K 1985 *Z. Phys. B* **58** 311
- [74] Albano E V 1993 *J. Phys. A: Math. Gen.* **25** 2557
- [75] Jensen I 1993 *Phys. Rev. Lett.* **70** 1465
- [76] Hinrichsen H 2000 *Adv. Phys.* **49** 815
- [77] Beardau M, Yelenin G, Karpowicz A, Ehsasi M, Christmann K and Block J M 1999 *J. Chem. Phys.* **110** 11551
- [78] Voigt C A and Ziff R M 1997 *Phys. Rev. E* **56** R6241
- [79] Muñoz M A, Dickman R, Vespignani A and Zapperi S 1999 *Phys. Rev. E* **59** 6175
- [80] Nettesheim S, von Oertzen A, Rotermund H H, and Ertl G. 1993 *J. Chem. Phys.* **98** 9977
- [81] Evans J W and Miesch M S 1991 *Phys. Rev. Lett.* **66** 833, 1991 *Surf. Sci.* **245** 401
- [82] Albano E V 2001 *Phys. Lett. A* **288** 73
- [83] Stauffer D 1991 *Introduction to the percolation theory* (London: Francis and Taylor)
- [84] Albano E V, Binder K and Paul W 1997 *J. Phys. A: Math. Gen.* **30** 3285
- [85] Dickman R and Tomé T 1991 *Phys. Rev. A* **44** 4833
- [86] Bidaux R, Boccara N, and Chaté H 1989 *Phys. Rev. A* **39** 3094

- [87] Albano E V 1992 *Appl. Phys. A* **55** 226
- [88] Brosilow B J and Ziff R M 1992 *Phys. Rev. A* **46** 4534
- [89] Meakin P and Scalapino D J 1987 *J. Chem. Phys.* **87** 731
- [90] Yaldran K and Sadiq A 1989 *J. Phys. A: Math. Gen.* **22** L925
- [91] Hua D-Y and Ma Y-Q 2002 *Phys. Rev. E* **66** 066103
- [92] Redhead P A 1962 *Vacuum* **12** 203
- [93] Chan C M and Weinberg W H 1978 *Appl. Surf. Sci.* **1** 377
- [94] Stanley H E 1971 *Introduction to phase transitions and critical phenomena* (New York: Oxford University Press)
- [95] Lee K J, McCormick W D, Ouyang K and Swinney H L 1993 *Science* **261** 192
- [96] Lee K J, McCormick WD, Pearson J E, and Swinney H L 1994 *Nature (London)* **369** 215
- [97] Zhabotinskii A M and Zaikin A N 1970 *Nature (London)* **225** 535
- [98] Winfree A T 1972 *Science* **175** 634
- [99] Turing A M 1952 *Philos. Trans. R. Soc. London B* **237** 37
- [100] Rose K C, Battogtokh D, Mikhailov A, Imbihl R, Engel W and Bradshaw A M 1996 *Phys. Rev. Lett.* **76** 3582
- [101] Edward S F and Wilkinson D R 1982 *Proc. Roy. Soc.(London) A* **381** 17
- [102] Chávez F, Vicente L, Perera A and Moreau M 1999 *J. Chem. Phys.* **110** 8118
- [103] Kang H C and Weinberg W H 1993 *Phys. Rev. E* **47** 1604
- [104] Moller P, Wetzl K, Eiswirth M and Ertl G 1986 *J. Chem. Phys.* **85** 5328
- [105] Kaukonen H P and Nieminen R M. 1989 *J. Chem. Phys.* **91** 4380
- [106] Brosilow B J and Ziff R M 1992 *Phys. Rev. A* **46** 4534
- [107] Albano E V 1992 *Appl Phys A* **55** 226
- [108] Luque J J, Jiménez-Morales J and Lemos M C 1992 *J. Chem. Phys.* **96** 8535
- [109] Satulovsky J and Albano E V 1992 *J. Chem. Phys.* **97** 9440
- [110] Leite V S, Figueiredo W 2002 *Phys. Rev. E* **66** 046102
- [111] Albano E V 1990 *Phys. Rev. B* **42** R10818
- [112] Albano E V 1990 *Surf. Sci.* **235** 351
- [113] Casties A, Mai J and von Niessen W 1993 *J. Chem. Phys.* **99** 3082
- [114] Mai J, Casties A and von Niessen W 1993 *Chem. Phys. Lett.* **211** 197
- [115] Mai J, Casties A and von Niessen W 1992 *Chem. Phys. Lett.* **196** 358
- [116] Albano E V 1992 *Phys. Lett. A* **168** 55
- [117] Jensen I 1991 *J. Phys. A: Math. Gen.* **24** L1111
- [118] Albano E V 1994 *J. Phys. A: Math. Gen.* **27** 431
- [119] Pereyra V D and Albano E V 1994 *J. Phys. A: Math. Gen.* **27** 7763
- [120] Tammaro M and Evans J W 1995 *Phys. Rev. E* **52** 2310
- [121] Cortés J and Valencia E 1997 *Surf. Sci.* L243
- [122] Khan K M and Albano E V 2002 *Chem. Phys.* **276** 129
- [123] Khan K M and Yaldran K 2000 *Surf. Sci.* **445** 186
- [124] Jensen I and Fogedby H C 1990 *Phys. Rev. A* **42** 1969
- [125] Mai J and von Niessen W 1990 *J. Chem. Phys.* **93** 3685
- [126] Evans J W 1993 *J. Chem. Phys.* **98** 2463
- [127] Mai J and von Niessen W. *Chem. Phys.* **156** 63
- [128] Meakin P 1990 *J. Chem. Phys.* **93** 2903
- [129] Lorenz D C, Haghgooie R, Kennebrew C and Ziff R M 2002 *Surf. Sci.* **517** 75
- [130] Hoenicke G L and Figueiredo W 2000 *Phys. Rev. E* **65** 8768
- [131] Valencia E, Cortés J and Pushmann H 2000 *Surf. Sci.* **470** L109
- [132] Hovi P J, Vaari J, Kaukonen H P and Nieminen 1992 *Comput. Mater Sci.* **1** 33
- [133] Egelhoff W F Jr 1982 *Fundamental Studies of Heterogeneous Catalysis* vol 4 ed King D A and Woodruff D P (Amsterdam: Elsevier)
- [134] Yaldran K and Khan M A 1991 *J. Catal.* **131** 369

- [135] Brosilow B J and Ziff R M 1992 *J. Catal.* **136** 275
- [136] Meng B, Weinberg W H and Evans J W 1993 *Phys. Rev. E* **48** 3577
- [137] Meng B, Weinberg W H and Evans J W 1994 *J. Chem. Phys.* **101** 3234
- [138] Dickman A G, Grandi B C, Figueiredo W and Dickman R, 1999 *Phys. Rev. E* **59** 6361
- [139] Loscar E S and Albano E V 2002 *Phys. Rev. E* **65** 066101
- [140] Kortlüke O, Kuzovkov V M and von Niessen W 1997 *Chem. Phys. Lett.* **275** 85
- [141] Khan M A, Yaldram K, Khalil G K and Khan K M 1994 *Phys. Rev. E* **50** 2156
- [142] Khan K M and Ahmad W 2002 *J. Phys. A: Math. Gen.* **35** 2713
- [143] Tammaro M and Evans J W 1998 *J. Chem. Phys.* **108** 7795
- [144] Albano E V 1992 *J. Stat. Phys.* **69** 643
- [145] Maltz A and Albano E V 1992 *Surf. Sci.* **277** 414
- [146] Yaldran K Khan K M Ahmed N and Khan M A 1993 *J. Phys. A: Math. Gen.* **26** 2663
- [147] Hui-Yun P, Jun W H and Sen Z Z *J. Phys. A: Math. Gen.* **28** 4279
- [148] Khan K M, Yaldram K and Ahmad A In press *J. Chem. Phys.*
- [149] Khan K M, Albano E V and Monetti R 2002 *Surf. Sci.* **481** 78
- [150] Khan K M and Ahmad N 2001 *Chem. Phys. Lett.* **339** 179
- [151] Khan K M, Ahmad N and Albano E V 2001 *Surf. Sci.* **494** 111
- [152] Albano E V 1994 *Surf. Sci.* **306** 240
- [153] Albano E V *J. Phys. A: Math. Gen.* **27** 3751
- [154] Albano E V 1995 *Physica A* **214** 426
- [155] Öhler J K and ben Avraham D 1991 *J. Phys. A.* **24**, L261.
- [156] ben Avraham D and Köhler J 1992 *J. Stat. Phys.* **65**, 839.
- [157] Khan K M, Basit A and Yaldram K 2000 *J. Phys. A: Math. Gen.* **33**, L215
- [158] Khan K M, Ahmad and Iqbal K 2002 *J. Phys. Condens. Matter* **14**, 7177
- [159] Harris T E 1974 *Ann. Prob.* **2** 969
- [160] Durrett R 1988 *Lecture Notes in Particle Systems and Percolation.* (Pacific Grove CA: Wadsworth)
- [161] Schlögl F 1972 *Z. Phys. B.* **253** 147
- [162] Monetti R and Albano E V 1995 *Phys. Rev. E* **52** 5825
- [163] Monetti R 2002 *Phys. Rev. E* **65** 016103
- [164] Takayasu H and Tretyakov 1992 *Phys. Rev. Lett.* **68** 3060
- [165] Jensen I (1993) *Phys. Rev. E* **47** R1
- [166] Domany E and Kinzel W 1984 *Phys. Rev. Lett.* **53** 311
- [167] Janssen H K 1981 *Z. Phys. B* **42** 151
- [168] Grassberger P 1982 *Z. Phys. B* **47** 365
- [169] Only few exceptions of DP are known so far. However, they all violate at least one of the essential conditions required for the validity of the DP conjecture, as discussed in Section 3.3. For some examples see reference [76].
- [170] Grassberger P 1997 *Nonlinearities in Complex Systems. Proceedings of the 1995 Shimal Conference on Complex Systems* (New Dehli: Narosa Publishing)